# High-pressure chemistry of nitride-based materials

**Elisabeta Horvath-Bordon,*[a] Ralf Riedel,*[a] Andreas Zerr,*[b] Paul F. McMillan,†*[c] Gudrun Auffermann,[d] Yurii Prots,[d] Welf Bronger,[d] Rüdiger Kniep*[d] and Peter Kroll*[e]**

*Received 22nd June 2006*
*First published as an Advance Article on the web 10th August 2006*
**DOI: 10.1039/b517778m**

Besides temperature at one atmosphere, the applied pressure is another important parameter for influencing and controlling reaction pathways and final reaction products. This is relevant not only for the genesis of natural minerals, but also for synthetic chemical products and technological materials. The present *critical review* (316 references) highlights recent developments that utilise high pressures and high-temperatures for the synthesis of new materials with unique properties, such as high hardness, or interesting magnetic or optoelectronic features. Novel metal nitrides, oxonitrides as well as the new class of nitride-diazenide compounds, all formed under high-pressure conditions, are highlighted. Pure oxides and carbides are not considered here. Moreover, syntheses under high-pressure conditions require special equipment and preparation techniques, completely different from those used for conventional synthetic approaches at ambient pressure. Therefore, we also summarize the high-pressure techniques used for the synthesis of new materials on a laboratory scale. In particular, our attention is focused on reactive gas pressure devices with pressures between 1.2 and 600 MPa, multi-anvil apparatus at $P < 25$ GPa and the diamond anvil cell, which allows work at pressures of 100 GPa and higher. For example, some of these techniques have been successfully upgraded to an industrial scale for the synthesis of diamond and cubic boron nitride.

## 1. Introduction

High-pressure is used so extensively in technology that it is almost impossible to catalogue the many ways in which our lives depend upon or are improved by it. From pneumatic tyres, household belongings and foodstuffs to advanced plastics, metals, ceramics and composite materials, there are countless materials that are fabricated, processed or shaped using high-pressure technology.

The modern era of high-pressure research and technology was ushered in with the work of P. Bridgman, who received the 1946 Nobel Prize in Physics for his pioneering experimental studies.[1,2] Bridgman's efforts were built upon by workers in the earth and mineral sciences, and by researchers seeking to reproduce the synthesis of diamond in the laboratory.[3–5,32] In recent years there have been rapid advances in both instrumentation and techniques, leading to a substantial growth in high-pressure science and technology. Stimulated by the quest to understand the structure and dynamics of the earth's deep interior and in the search for new materials, a combination of laboratory-scale diamond anvil cells (DACs) and "large-volume" synthesis presses, including apparatus designs such as belt, multi-anvil, toroidal and piston-cylinder,

[a]*Disperse Feststoffe, Material- und Geowissenschaften, Technische Universität Darmstadt, Petersenstraße 23, 64287 Darmstadt, Germany. E-mail: bordon@materials.tu-darmstadt.de; riedel@materials.tu-darmstadt.de*
[b]*Laboratoire des Propriétés Mécaniques et Thermodynamiques des Matériaux—CNRS, Institut Galilée, Université Paris 13, 99 av. J. B. Clement, 93430 Villetaneuse, France. E-mail: zerr@lpmtm.univ-paris13.fr*
[c]*Christopher Ingold Laboratories, Department of Chemistry, University College London, 20 Gordon Street, London, WC1H 0AJ, UK. E-mail: p.f.mcmillan@ucl.ac.uk*
[d]*Max-Planck-Institut für Chemische Physik fester Stoffe, Anorganische Chemie, Nöthnitzer Straße 40, 01187 Dresden, Germany. E-mail: kniep@cpfs.mpg.de*
[e]*Institut für Anorganische Chemie, RWTH Aachen, Professor-Pirlet-Straße 1, 52056 Aachen, Germany. E-mail: peter.kroll@ac.rwth-aachen.de*
† Also at: Royal Institution of Great Britain, Davy–Faraday Research Laboratory, 21 Albemarle Street, London, W1S 4BS, UK. E-mail: paulm@ri.ac.uk

**Elisabeta Horvath-Bordon**

*Elisabeta Horvat-Bordon has been scientific assistant in the Department of Dispersive Solids, Material Science at Darmstadt University of Technology, Germany since 2006. She received her PhD in materials science in 2004 from Darmstadt University of Technology with the thesis "Synthesis and Characterisation of Carbon Nitride". Between 2004 and 2006 she was scientific assistant at the Institute of Chemical Materials Science at the University Konstanz, Germany and the Institute of Inorganic Chemistry at the TU Bergakademie Freiberg, Germany. She graduated in 1996 in Industrial Chemistry from Babes-Bolyai University, Cluj-Napoca, Romania. Her current research interest is focused on the ultra-high-pressure synthesis of new materials.*

are being applied in laboratories around the world to explore the structural chemistry, bonding and reactions of crystalline and amorphous solids and liquids under high-pressure conditions.[6,7] These investigations in "static" high-pressure science are complemented by the "dynamic" shock-wave experiments generally carried out in large-scale facilities. Dynamic high-pressure and temperature conditions can be achieved by applying projectile impact on the initial sample by explosions or laser shock, or by discharging large quantities of electrical or magnetic energy into the sample chamber.[8,9] The shock-wave experiments provide the most extreme high-pressure and high-temperature conditions. Pressures into the multi-megabar range (>1 000 000 atm or several hundred GPa) and extending up to 50 TPa (50 000 GPa), with simultaneous heating to thousands or tens of thousands of °C, can be achieved. Shock wave techniques enable the synthesis of new materials, and samples can be recovered for study under ambient conditions.[10,11,78] However, the methods are expensive and they must be carried out in the context of a large facility. Also, the transient pressurization only lasts for a matter of milliseconds to microseconds and it is difficult to obtain detailed structural information on the compressed sample.

At the other end of the scale there is the hand-held DAC, in which the sample is compressed between the flattened tips of two gem-quality diamonds. A DAC allows ready access to the 100 GPa (megabar) regime (1 Mbar = 100 GPa). Resistive- and laser-heating techniques enable controlled simultaneous

**Ralf Riedel**

*Professor Riedel gained his PhD in Inorganic Chemistry in 1986. Between 1986 and 1992 he joined the Max-Planck-Institute for Metals Research and the Institute of Inorganic Materials at the University of Stuttgart, Germany. In 1992 he finished his Habilitation in Inorganic Chemistry. Since 1993 he has been Professor at the Institute of Materials Science at Darmstadt University of Technology. Professor Riedel is a Fellow of the American Ceramic Society and was awarded the Dionyz Stur Gold Medal for his merits in the natural sciences. He is a member of the World Academy of Ceramics and Guest Professor at Jiangsu University in Zhenjiang, China. His current research interests are focused on (i) polymer derived ceramics and (ii) ultra-high-pressure synthesis of new materials.*

**Andreas Zerr**

*Andreas Zerr is a CNRS researcher at the Laboratoire des Propriétés Mécaniques et Termodynamiques des Matériaux, Université de Paris XIII. He received his Diploma in Experimental Physics in 1988 from the Moscow Institute of Physics and Technology—State University. The research for his Diploma was carried out at the Institute for High-Pressure Physics of the Russian Academy of Sciences. In 1991 he started doctoral work in the High-Pressure Mineral Physics Group at the Max-Planck-Institute for Chemistry in Mainz, Germany, lead by Dr. R. Boehler, and received his doctorate from the Johannes Gutenberg University, Mainz in 1995. Until 1997 his research was supported by a stipend of the Max Planck Society. His studies at Mainz concentrated on investigations of the structural and melting behaviour of minerals and rocks at high pressures and temperatures using the laser heated diamond anvil cell technique. From 1997 to 2005 he was employed as a research scientist in the Disperse Solids Group in the Department of Material- and Geo-Sciences at Darmstadt University of Technology, lead by Prof. R. Riedel. Since then he has explored paths for the synthesis of novel advanced nitrides at high pressures and temperatures.*

**Gudrun Auffermann**

*Gudrun Auffermann has worked as a scientist (head of competence group analytics) at the Max-Planck-Institute for the Chemical Physics of Solids in Dresden, Germany since 1998. She received a Diploma degree in chemistry (1984) and obtained her PhD (1987) with Professor Welf Bronger at the RWTH Aachen, Germany on the synthesis and characterisation of ternary metal hydrides. This was followed by postdoctoral research at the RWTH Aachen with Professor Welf Bronger (1987–1996) and the Max-Planck-Institute for Solid State Research, Stuttgart with Professor Arndt Simon (1996–1998). Her main interests are reactive gas pressure syntheses of nitrogen- and hydrogen-containing materials, structural studies and analytics.*

**Yurii Prots**

*Yurii Prots has worked as a scientist at the Max-Planck-Institute for the Chemical Physics of Solids in Dresden since 1999. He received a Diploma degree in chemistry in Lviv, Ukraine (1991) and obtained his PhD (1998) with Professor Wolfgang Jeitschko at the University of Münster, Germany on the structure and properties ternary silicides. His main interests are in structural studies of intermetallic compounds and the synthesis of nitrogen-containing compounds at high-pressure.*

heating of samples from a few hundred up to several thousand degrees while they are being held at high-pressure.

Most experiments in solid state chemistry that lead to technologically useful materials are carried out under pressure conditions close to ambient ($P$ = 1 atm), using mainly variable temperatures combined with chemical composition to explore the range of available compounds and their properties. The use of high pressures, combined with high temperatures and compositional variables, provides an opportunity to synthesize entirely new classes of materials and/or to tune their electronic, magnetic and structural properties for a wide range of applications. Synthetic diamond and the cubic phase of boron nitride, c-BN, are the hardest known solids, were the first industrially synthesized high-pressure materials and are still in use today for a wide range of cutting and grinding applications.[12] High-pressure and high-temperature research to improve the synthesis and processing methods for diamond and c-BN is still on-going, as are studies to establish new "superhard" materials that have mechanical properties and chemical and thermal resistance comparable-with or superior-to those of diamond and c-BN phases.[13,14] New materials explored and synthesized using high-pressure techniques include binary nitrides with spinel ($Si_3N_4$, $Ge_3N_4$) and thorium phosphate ($Zr_3N_4$, $Hf_3N_4$) structures. The high-pressure nitrides possess high hardness, and the new polymorphs of $Si_3N_4$ and $Ge_3N_4$ have a wide direct band gap between 3.0–4 eV, comparable to the newly-developed UV/blue light emitting diode materials based on Al, Ga and In nitride.[15,16]

Most studies in materials chemistry and high-pressure research have focused on oxides, which have provided the largest group of inorganic compounds leading to technologically important materials. Research on superhard materials has centred around variations on the diamond theme, with exploration of new compounds in the B–C–N–O system, some of which have been discovered and are synthesised under high-pressure, high-temperature conditions. There is another grand family of high hardness materials among the carbides and nitrides of transition metals, including WC, TiN, *etc*. These materials also provide metallic materials with useful electronic and magnetic properties, and can be superconducting, with high values of $T_c$ (NbN, MoN). The solid state chemistry of nitrides has been relatively neglected compared to that of oxide compounds, although there has been considerable activity in the area over the past two decades.[17–19] Many new nitride compounds with novel physical and chemical properties have attracted attention as potential technological materials. For this reason, we focus in this review on the high-pressure materials chemistry of nitrides and related phases, including nitride-imides, oxonitrides and azo compounds. We present

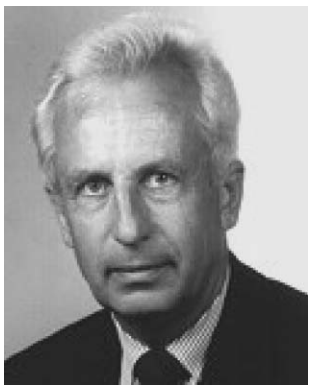

**Welf Bronger**

*Welf Bronger studied chemistry at the universities of Innsbruck, Austria and Münster, Germany and gained his PhD in 1969 supervised by Wilhelm Klemm. After a short period working in industry for Degussa, he returned to the University of Münster as an assistant, where he received his Habilitation in 1966. In 1969 he took up the chair of Inorganic and Analytical Chemistry at the RWTH Aachen. Since his retirement in 1997, he has continued his research in collaboration with the Max-Planck-Institute for the Chemical Physics of Solids in Dresden. His main research interests are concerned with intermetallic phases, metal chalcogenides and metal hydrides, with special emphasis on structural studies and magnetochemistry.*

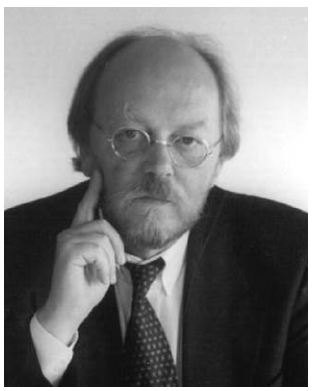

**Rüdiger Kniep**

*Rüdiger Kniep has been the Director and a Scientific Member of the Max-Planck-Institute for the Chemical Physics of Solids in Dresden since 1998. He received Diploma degrees in chemistry (1970) and mineralogy (1971) at Braunschweig Technical University, Germany. His dissertation work was done with Professor Albrecht Rabenau at the Max-Planck-Institute for Solid State Research in Stuttgart (1973). After post-doctoral research and a professorship (1979) at the University of Düsseldorf, Germany, he moved to Darmstadt Technical University (full professorship 1987, Eduard Zintl Institute). He is most widely known for his work on solid state chemistry, biomineralisation and structure–property relationships of solid materials.*

**Peter Kroll**

*Peter Kroll currently holds a Heisenberg-fellowship of the German Science Foundation. He received his Diploma degree in physics (1993) at Ruprecht-Karls-University Heidelberg with a thesis work in Theoretical Elementary Particle Physiscs. He moved to Darmstadt University of Technology for his PhD, joining the group of Ralf Riedel in the Department of Materials Science. His dissertation from 1996 was devoted to experimental characterization and structural modelling of amorphous silicon nitride ceramics. He did his post-doctoral research in the Department of Chemistry and Chemical Biology at Cornell University together with Roald Hoffmann until 1999, when he joined the Department of Inorganic Chemistry at RWTH Aachen. In 2005 he finished his habilitation in Inorganic Chemistry and received the venia legendi. He is eagerly pursuing a computational science approach to solid dstate chemistry: His interests include amorphous and nanostructured materials as well as high-pressure phase transformations and new compounds.*

the results of recent research on several binary, ternary and quaternary materials including C–N, Si–N, Ge–N, Sn–N, Zr–N, Hf–N, Mo–N, Si–Ge–N, Si–C–N, B–C–N, Si–O–N, Al–O–N, Ga–O–N, Si–Al–O–N and related systems. These compounds are expected to show a unique combination of high hardness, oxidation resistance and chemical inertness, along with useful electronic, magnetic and optoelectronic properties.[20,21] It is predicted that different high-pressure phases can be used as high-temperature or optically-active semiconductors because of their variable band gap.[12]

In parallel with the rapid development of experimental techniques, tremendous advances have been made in the theory and computation of materials in the past few decades, often driven by the needs and results of high-pressure materials science. Especially with the advent of density functional methods and the widespread availability of powerful and inexpensive computers, it has become possible to calculate reliably and efficiently the structure and energy of existing and hypothetical phases on a relatively routine basis. For example, a problem containing several dozen atoms within the unit cell can now be treated readily using a desktop computer, and with a parallel supercomputer that can be implemented either at national or international facilities, or enabled by networking desktop PCs, a manifold of structural approximants can be investigated at almost any level of accuracy and pressure–temperature condition.

In the mutual interplay between problem generation and problem solving involved in high-pressure and temperature research, experiment and computation play a constant game of ''leap-frog'': sometimes the experiment is in advance of theory and sometimes the computation provides a theoretical prediction that must be tested experimentally. In most studies, the two evolve simultaneously and in close collaboration. Therefore, the use of high-pressure synthesis and *in situ* characterization methods combined with theory are indispensable to predict, test and confirm the presence of a new high-pressure compound or structure and its potentially useful material properties.

The present review highlights current research in the field of materials chemistry, including exploration, synthesis and characterization of likely new technological compounds under extreme high-pressure and temperature conditions. As high-pressure techniques, we discuss (i) reactive high-pressure devices, (ii) multi-anvil apparatus (MA) and (iii) DAC. In particular, we focus our attention on the scientific efforts and issues associated with the synthesis, structure, properties, processing and modelling of novel nitrides and oxonitrides of elements within groups 13 and 14, as well as transition metal nitrides.

## 2. High-pressure methods

### 2.1 Reactive gas pressure devices

The design and development of the reactive gas pressure devices described in the following paragraphs established solid state reactions in the pressure range between 1.2 and 600 MPa, and with different gases, *e.g.* $H_2$, $N_2$ and Ar.[22,23] All the loading and unloading procedures of the autoclaves are carried out under an inert gas atmosphere (argon glove boxes) in order to protect all materials against impurities. This special equipment for the syntheses and handling of samples under high purity conditions and a protective atmosphere is closely related to the general progress made in the area of solid state chemistry.

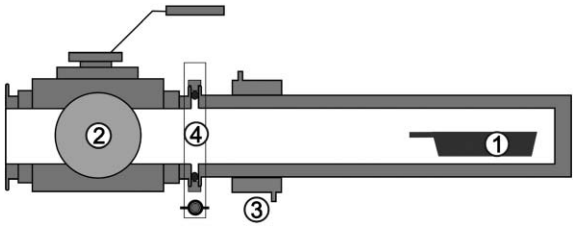


**Fig. 1** Schematic sketch of the pressure autoclave (1–12 bar). (1) Reaction boat; (2) Ball valve; (3) Cooling jacket; (4) Flange connection with trapped centring O-ring.

Reactive gas pressure experiments, up to 12 bar reaction pressure, are carried out in the pressure device shown in Fig. 1 and Fig. 2. The autoclave, made of ATS-340 steel, is closed by the use of a ball valve before being connected *via* a flange to the low pressure equipment (Fig. 2) outside the box. The whole system is evacuated to $10^{-6}$ bar and thereafter filled with $N_2$ (99.999%, purified by Oxisorb-cartridges, Messer Griesheim) to a starting pressure maximum of 10 bar, followed by heating up to the desired reaction temperature. The progress of a reaction can be followed by using a pressure gauge.

Pressure experiments up to 6000 bar are carried out in the pressure device shown in Fig. 3 and Fig. 4. The autoclave (Fig. 3) is closed with a copper gasket (3), which is placed in a back-up ring and fitted to the inner ram cylinder connected to a high-pressure valve (2). Afterwards, the autoclave is closed by using threaded studs. The female screws are tightened as much as possible in the glove box and finally tightened outside the box with an adjustable torque wrench up to 140 Nm. Next, the autoclave is fitted to the high-pressure equipment (see Fig. 4). The whole system is evacuated to $10^{-6}$ bar and filled up with nitrogen gas up to the desired starting pressure (room temperature). Pressures higher than 200 bar (above gas bottle pressure) can be obtained by using the following procedure: The medium pressure storage vessels (9) are cooled with liquid

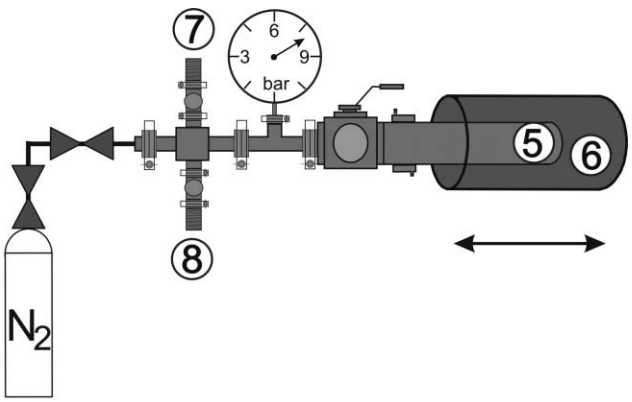


**Fig. 2** Schematic sketch of the pressure equipment (1–12 bar). (5) Low pressure autoclave (see Fig. 1); (6) Furnace; (7) Connection to vacuum; (8) Connection to argon.

 

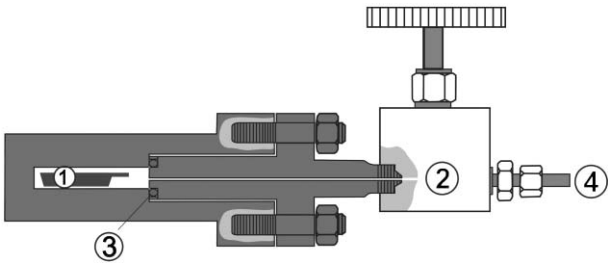


**Fig. 3** Schematic sketch of the high-pressure autoclave (up to 6000 bar). (1) Reaction boat; (2) High-pressure valve; (3) Copper gasket in a back-up ring; (4) High-pressure tube connection to the pressure equipment (see Fig. 4).

nitrogen and the gas is condensed up to a maximum 200 bar pressure. The medium pressure vessel is thawed to room temperature, the high-pressure autoclave is cooled down with liquid nitrogen and the reaction gas is condensed from the gas bottles into the autoclave. To achieve the highest pressure, a second autoclave (5) (all autoclaves are connected in series) is pre-cooled in an analogous manner, and the medium pressure vessel cooled again and filled with nitrogen. Then, the reaction autoclave (6) is cooled and filled step-by-step with nitrogen from the gas bottle, the medium pressure vessels (9) and the second autoclave (all three systems are at room temperature). This technology allows the reaction pressure in the autoclave to be set to the desired value (the maximum pressure is defined by the materials and the construction of the high-pressure equipment). The reaction volume of the autoclave is about 14 $cm^3$. The valves which are next to the autoclaves are water-cooled (8) during the heating process. The reaction pressure is measured and registered during the synthesis. After the reaction is finished, the autoclave is cooled down to room temperature. The autoclave is detached from the high-pressure equipment and the female screws are released slightly before the autoclave is transferred into the glove box, wherein the autoclave is unloaded. The copper gasket can easily be removed with a three-jaw adjustable puller in order to prepare the autoclave for the next experiment.

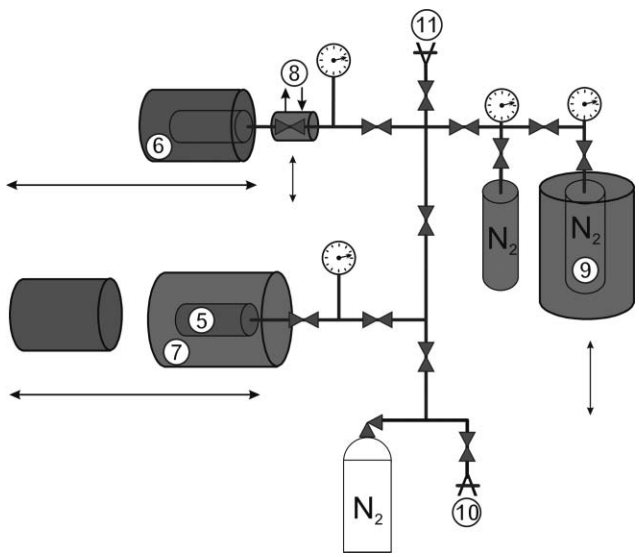


**Fig. 4** Schematic sketch of the high-pressure equipment (up to 6000 bar). (5) High-pressure autoclave (see Fig. 3); (6) Furnace; (7) Dewar for cooling the autoclave with liquid nitrogen; (8) Cooling jacket; (9) Medium-pressure storage vessels; (10) Connection to vacuum; (11) Gas outlet.

### 2.2 Multi-anvil apparatus

Generating the wide range of high-pressure and high-temperature conditions for materials exploration and synthesis covers a selection of dynamic and static compression techniques. On the one hand, extreme high-pressure and temperature conditions can be generated simultaneously by dynamic shock-wave compression with a time duration in the microsecond range. However, high-pressure conditions at relatively low temperatures cannot be realised by this dynamic method. In contrast, static compression is stable for a longer time at controllable temperature and pressure conditions, though the maximum pressure attainable is limited by the strength and design of the vessel. A convenient device for working in a lower pressure range (4–6 GPa) was the piston apparatus developed by Boyd and England.[24] This device had a tungsten carbide (WC) supported core and a very large sample chamber (several cubic centimetres). The synthesis of large samples is required for the study of magnetic properties, electrical conductivity, viscosity, thermal and mechanical properties. Beyond the limit of the piston cylinder ($\sim$maximum 6 GPa) and Belt apparatus ($\sim$maximum 10 GPa), multi-anvil devices can be used for reaching pressures exceeding 25 GPa.[31,32] By using large sintered diamond anvils instead of tungsten carbide, the higher pressure limit can be extended.[25–27] However, in the field of static compression, the highest pressure and temperature regimes can only be generated with a laser heated DAC (see below).

The evolution of multi-anvil devices has been reviewed in several articles and books.[28–36] The reachable pressure depends on the geometrical design of the devices, the frictional strength of the gasket and the compression strength of the anvil. Developments and improvements in this area led to several designs of anvil devices. Early designs for high-pressure generation were developed by Bridgman.[1,2] In fact, there are two basic types: the Bridgman opposed-anvil and multiple symmetrical anvils, as well as their variations.

The principle of a Bridgman opposed-anvil apparatus relies on compressing the sample between supported WC anvils. In this design, the maximum pressure depends on the cone angle ($\alpha$) and the compressive strength of the WC anvils. Generally, a $\alpha = 5^\circ$ cone angle and a compressive anvil strength of 5 GPa will generate pressures up to 20 GPa in the Bridgman geometry.

Essentially, in multi-anvil systems, a sample volume is compressed between variable numbers of identically shaped anvils in two stages, which move each other forward. The multi-anvil apparatus simply consists of a hydraulic press. The applied uniaxial loads can vary. In standard experiments this can be between 600 and 1000 tons, and in particular cases at 5000 tons *e.g.* at the Bayerisches Geoinstitut, Bayreuth, Germany.[37]

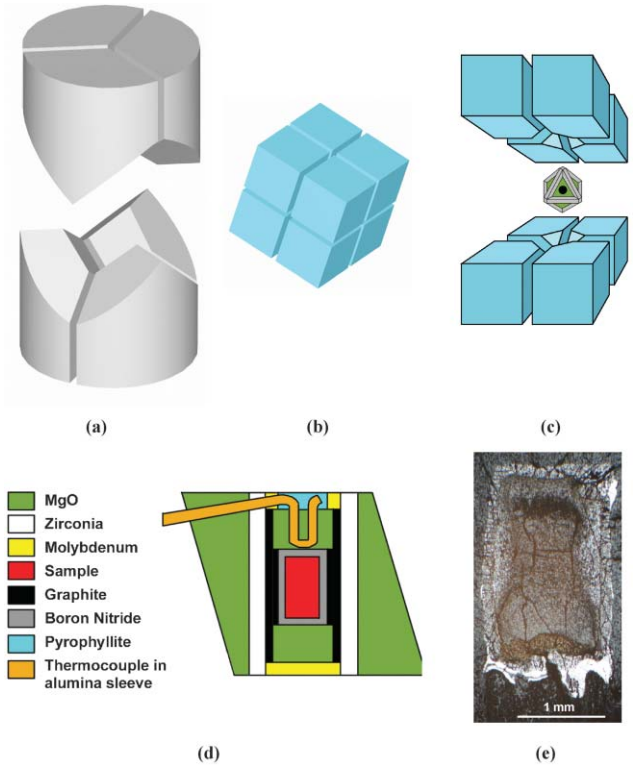


**Fig. 5** Details of the multi-anvil apparatus: (a) Walker-type module; (b) Eight WC cubic anvils; (c) Schematic of the compression of the octahedral pressure cell between the eight truncated WC anvils; (d) Cross-section of the octahedral pressure cell; (e) Cross-section of the sample.

The Walker-type multi-anvil press is based on a split cylinder geometry, in which six wedges (three at the top and three at the bottom) define an inner cubic cavity, as shown in Fig. 5a. The eight second-stage WC inner anvils, with truncated corners, are placed in the cubic cavity (Fig. 5b and 5c). The truncated corners form triangular faces with a different edge length. The pressure cell is placed in the octahedral cavity, which is formed by the eight WC cubes with truncated corners. The sizes of the truncation edge length (TEL: 3, 4, 5, 8, 11, 12 mm) of the WC cubes and the octahedral edge length (OEL: 7, 10, 14, 18, 19) of the pressure cell determine the sample volume and the reachable pressure range. The sample assembly is introduced into a cylindrical hole drilled into the octahedral pressure cell, which is made from semi-sintered $MgO–5\%Cr_2O_3$ ceramic. The sample assembly, depicted in Fig. 5d and 5e, shows the sample, the sample capsule, the resistance furnace, the thermocouples and the ceramic spacers. The temperature of the sample is usually determined by W–Re or Pt–Rh-based thermocouples and the pressure is derived from the applied load. Prior to the actual experiments, pressure calibration is performed by press-load experiments based on room temperature and high-temperature phase transitions of well-known materials (metals, minerals, *etc.*).

The multi-anvil method allows the synthesis of samples up to a few cubic millimeters in volume, while the DAC device can only produce sample volumes of a few cubic micrometers. However, the sample chamber within the multi-anvil is only partially accessible for *in situ* measurements, including high energy X-ray synchrotron diffraction and imaging studies. In contrast, the DAC readily allows a variety of *in situ* experiments, including laboratory-based optical spectroscopy.

### 2.3 Laser heated diamond anvil cell

It has been clearly demonstrated that the laser heated diamond anvil cell (LH-DAC) technique provides a powerful reconnaissance method for the synthesis and exploration of new promising high-pressure materials. Syntheses can be performed over an extremely wide range of pressures and temperatures; up to a few hundred GPa and a few thousand degrees Kelvin, for example. Under these extreme high-pressure conditions, novel bonding patterns, high coordination numbers and higher oxidation states for elements with multiple valances (*e.g.* iron, zirconium, or cerium) become favored, so that not only the production of new polymorphs of known compounds can be achieved, but also the synthesis of new compounds with stoichiometries not accessible at atmospheric pressure.[38,39] This is especially true when high-pressure and temperature synthesis is combined with the use of chemical precursors and unusual mixtures of elements. The materials obtained can be examined *in situ* at high-pressure, as well as after recovery, using different spectroscopic and diffraction methods. The range of techniques now in existence, including advanced microbeam techniques available at synchrotron sources, allow us to gain information on the structure and chemical composition of synthesized phases and compounds, even for samples of only a few tens of micrometers in size, typical of syntheses carried out in a LH-DAC. Moreover, electrical and mechanical properties, of potential interest for developing industrial applications, can now be determined experimentally for such small samples, especially using nano-probe techniques.[147]

The DAC was invented in 1959 by scientists at the University of Chicago and at the National Bureau of Standards (USA) with the initial aim of studying X-ray diffraction and the infrared (IR) spectra of solids *in situ* at high pressures.[40–42] This new technique revolutionized the development of high-pressure research, since it led to a significant extension of the pressure region where the physical and chemical behavior of condensed matter could be investigated, and it enabled the *in situ* observation and diffraction (or spectroscopic characterization) of samples under high-pressure conditions. Today, static pressures in excess of 500 GPa are reported to be attainable at room temperature using this technique.[43] A large variety of DACs are now available, all of which are based on the same principle of opposed anvil technology for pressure generation but differ in the methods used for anvil alignment, load generation and sample mounting.[44–46,30] A great advantage of the DAC technique is the remarkable transparency of diamond to light over a broad spectral range: from far IR to near ultraviolet and to X-ray radiation for $\lambda < 1$ Å.[45–48] This allows *in situ* sample analysis to be carried out at high pressures by various different spectroscopic techniques, including Raman and Brillouin scattering, IR, UV-visible absorption spectroscopy, X-ray

 

absorption, emission and fluorescence spectroscopy, γ-ray spectroscopy (*i.e.*, Mossbauer), or by X-ray diffraction and scattering experiments. The structure of recovered metastable samples can be determined at a micro- to a nanoscale by electron diffraction and imaging techniques using transmission electron microscopy (TEM). Chemical composition can be obtained using X-ray fluorescence techniques such as EDX-spectroscopy or electron microprobe analysis, or electron energy loss spectroscopy (EELS). The development of the convenient ruby pressure scale, where the red shift of the $R_1$-fluorescence line of ruby with pressure is used for pressure determination, led to practical applications of the DAC techniques.[49–51]

The high transparency of diamond to IR and near-IR light[40,41] allows the heating of samples in a DAC through the absorption of focused intense laser radiation; the method first being implemented by Ming and Bassett,[52] who used a pulsed ruby laser and also a continuous-wave (cw) Nd:YAG (yttrium–aluminum–garnet) laser to heat samples in a DAC to above 3300 K and 2300 K, respectively. Today, two types of continuous-wave IR lasers are extensively used for sample heating: solid state Nd:YAG lasers (or Nd:YLF, yttrium–lithium–fluorite), with the most intense line at a wavelength of $\lambda$ = 1.064 μm (or 1.054 μm for Nd:YLF lasers), and $CO_2$ gas lasers, with the most intense line at $\lambda$ = 10.6 μm. The Nd:YAG (or Nd:YLF) lasers are used for heating semiconductors[53] and metals, as well as insulators containing transition metals such as Fe, Ni, *etc*.[52] The $CO_2$ laser heating technique, first employed by Boehler and Chopelas,[54] has been used in experiments on numerous non-conducting inorganic (oxides, silicates, nitrides *etc.*) and organic materials.[55–58] Continuous development of the LH-DAC technique now allows temperatures to be achieved that are not attainable by any other static high-pressure technique. The maximum values reported in the literature for both laser types, Nd:YAG (or Nd:YLF) and $CO_2$, today approach 7000 K.[57–59]

In experiments with the LH-DAC, temperatures developed within the sample chamber can be determined from the thermal radiation of heated samples $I_{RB}(T, P, \lambda)$ measured in the visible and near-IR wavelength region (400 nm to 1600 nm). Temperature is obtained by fitting a product of Planck's formula and emissivity $\varepsilon(T, P, \lambda)$, which is, in general, a wavelength-, pressure- and temperature-dependent function, to the measured emissivity spectrum (eqn. 1):

$$I_{RB}(T,P,\lambda) = \varepsilon(T,P,\lambda) \times I_{BB}(T,\lambda) = \varepsilon(T,P,\lambda) \times \frac{8\pi hc}{\lambda^5} \times \frac{1}{(e^{hc/\lambda kT} - 1)} \quad (1)$$

Here $h$ is Planck's constant, $k$ the Boltzmann constant, $c$ the velocity of light in a vacuum, $T$ the absolute temperature and $\lambda$ the wavelength. Planck's formula[60] describes the temperature and wavelength dependence on the thermal radiation intensity of the black body (BB), $I_{BB}(T,\lambda)$. Emissivity is always less than unity, indicating the deviation of thermal radiation in a real body (RB) from that of a hypothetical BB.[48] Since there is as yet no reliable method to estimate the change of the wavelength-dependences on emissivities at high pressures and temperatures, and experimental data are scarce, this characteristic material property is usually assumed to be wavelength-independent. Such assumptions can result in errors in temperature determination approaching a few hundred degrees Kelvin in LH-DAC experiments.[57,59,61,62]

However, although the unknown wavelength-dependences of emissivities at high pressures and temperatures provide almost an inevitable source of errors, there are other experimental details that can cause even larger avoidable errors in temperature determination. A long-standing subject of debate was the question of whether a reliable measurement of temperature in a LH-DAC was possible when thermal radiation spectra were collected using refractive optics.[56,61,63–69] In contrast to reflecting optics, the spectral intensities of spectra collected using refractive optics are biased by chromatic aberrations that can cause temperature errors of 100% or more.[70] The current state of the debates on this matter is remarkable.[71,72] It now appears that the use of refractive optics for temperature measurements in a LH-DAC can only be tolerated when temperature gradients in the examined sample area are negligible and sharp sample images have to be obtained during the experiments. However, temperature gradients can only be minimized in the center of the heated spot by using high power lasers and by incomplete focusing of the heating laser beam on the sample surface. Thermal isolation of samples from the diamond anvils allows a more effective use of the laser radiation, as well as a reduction of the axial temperature gradients.

The design of a sample assemblage in a LH-DAC depends on the aim of the particular experiment. Two examples are shown schematically in Fig. 6. The sample container is made by drilling a hole in a pre-indented metal gasket (typical dimensions: 150 μm diameter and 50–60 μm height). The samples, which could be single crystals, glass chips or pressed powder pellets (typical dimensions of about 70 × 70 × 15 μm), can be isolated from the highly thermally conducting diamond anvils using small grains of the sample material (Fig. 6a) or a layer of alkali halides (for example NaCl or KBr) (Fig. 6b). The samples can also be embedded in pressure transmitting media such as Ar or $N_2$. Depending on the chemical composition of samples and the intended temperature conditions,

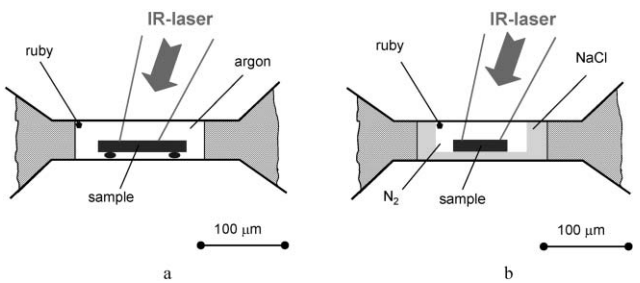


**Fig. 6** Schematic drawings of sample assemblages in a LH-DAC. The sample is heated with the radiation of an IR laser. (a) Argon, neon or helium can be used as pressure media when chemically inert and/or quasi-hydrostatic loading conditions are required. (b) Nitrogen should be used as a pressure medium in experiments on nitrides to preclude their decomposition. In experiments on the synthesis of nitrides from elements, the nitrogen pressure medium also served as a reactant source. The fluorescence of ruby crystals can be excited using an Ar laser.

different pressure media are chosen. To provide quasi-hydrostatic pressure conditions and/or a chemically inert environment, an argon, neon or helium pressure medium can be used. Alkali halides, which are less hydrostatic and less chemically inert, are however better thermal isolators and do not require the use of gas loading devices. Nitrogen (which is a solid above 2.3 GPa at room temperature)[73] can be used in experiments on nitrides to ensure their chemical stability at high temperatures, by providing a high $N_2$ chemical potential.[55,74,75] The possibility of using nitrogen as a pressure medium in a LH-DAC also makes this technique ideally suited for the synthesis of new nitrides.[77,182,183] This allows the use of nitrogen-free starting materials (*e.g.* elemental metals and their alloys) or materials with a low nitrogen content (*e.g.* mononitrides, ZrN or HfN) in synthesis. Such an option is of particular importance when starting materials of the required stoichiometry are not available and/or if their preparation at ambient pressure is very difficult. Additionally, high nitrogen pressures significantly extend the kinetic and thermodynamic stability of nitrides at high temperatures. This phenomenon is of tremendous importance for the synthesis of new covalent nitrides because high temperatures allow kinetic barriers to be overcome and phase transitions or chemical reactions to be accelerated to reasonable rates. Sample contamination does not take place for nitride samples in a DAC embedded in a high purity nitrogen pressure medium, heated with IR laser radiation. In the pressure medium, temperatures decrease rapidly from those on the surface of the heated sample to nearly room temperature on the diamond anvil surface.[76] A pressure transmitting medium with such a strong temperature gradient works as a chemically uniform capsule, isolating the sample from the environment. As nitrogen can be easily substituted by oxygen, special attention should be paid to the elimination of possible oxygen sources from the reaction volume. One of the typical ways that oxygen (in form of water/ice) is introduced into the reaction volume in a LH-DAC is by the use of impure commercial liquid nitrogen, or by cryogenic loading of pure liquid nitrogen from the laboratory air atmosphere.

The only significant disadvantage of the LH-DAC technique is the extremely small size of the synthesized samples, which are usually in the order of 20–50 μm. However, such small sample amounts can be reliably characterized using microbeam and nanoscale techniques, including optical spectroscopy, diffraction and electron microscopy[55,77]

In summary, from the point of view of materials chemistry, a LH-DAC provides a very wide pressure and temperature range for the synthesis of new materials and phases, some of which can be recovered metastably under ambient conditions. The heating of different element combinations at high pressures in a LH-DAC can result in the formation of new compounds that are not accessible *via* any other ambient- or high-pressure technique, including shock compression. In contrast to shock compression techniques, in which samples are subjected to high pressures and temperatures for only about one microsecond,[78] samples in a LH-DAC can be subjected to the desired pressure–temperature conditions for long periods (*e.g.*, up to a few hours). Last, but not least, a great advantage of LH-DACs are the lower investment and operational costs compared to shock compression techniques and even large volume multi-anvil devices (the static HP-HT apparatus with next accessible pressure and temperature maxima of about 25 GPa and 3000 K, respectively). For seeking new materials, the LH-DAC is highly time efficient and cost effective compared to other techniques. For example, synthesis experiments in a multi-anvil device require long periods of time for the compression (a few hours) and especially the decompression (up to 12 h) of a sample, even if, at high pressures, the samples are to be heated only for a few minutes. In contrast, for a LH-DAC, the experiment duration (typically below 1 h) is defined by the time needed for the alignment of the laser beam and for sample heating.

## 3. Nitrides

### 3.1 Binary and ternary main group element nitrides

The most explored high-pressure phase in the $A_3N_4$ family is the carbon nitride, $C_3N_4$. Research in this field was initiated by theoretical predictions in the 1980s that saturated $sp^3$-hybridised carbon(IV) nitride phases, in particular a β-$C_3N_4$ phase with the β-$Si_3N_4$ structure, should be as hard as or even harder than diamond.[79–81] In addition to the potential β-$C_3N_4$, the existence of other α-, pseudocubic, cubic and graphitic polymorphous carbon nitride phases have been suggested on the basis of calculations.[82–84,113]

Structural data of the hypothetical $C_3N_4$ phases, together with their calculated bulk moduli, are arranged in Table 1. During the 1990s, the number of publications related to CVD and PVD synthesis approaches to $C_3N_4$ increased exponentially. The theoretical and experimental results of the $C_3N_4$ research were summarized and analyzed in several review articles.[85–90]

Numerous experimental attempts to synthesize carbon nitride in any structural form have exploited various synthetic methods (Fig. 7), such as chemical (CVD) and physical (PVD) deposition techniques, and static (MA, DAC) and dynamic (shock compression) high-pressure methods.[91–97,121,126] The synthesis of carbon nitride precursors adopt several routes. The most common of these are solid state metathesis reactions, successfully applied to the synthesis of lanthanides and transition metals nitrides, and the solvothermal route, used for the efficient preparation of GaN.[98–103] Furthermore,

**Table 1** Predicted $C_3N_4$ phases (B = the calculated bulk modulus, $\rho$ = the calculated density)

| Modification | Space group | *a*/Å | *c*/Å | *β*/° | $\rho$/g cm$^{-3}$ | *B*/GPa | Ref. |
|---|---|---|---|---|---|---|---|
| α-$C_3N_4$ | $P3_1c$ (159) | 6.35 | 4.46 | — | 3.78 | 189 | 84 |
| α-$C_3N_4$ | $P3_1c$ (159) | 6.47 | 4.71 | — | 3.58 | 425 | 82 |
| α-$C_3N_4$ | $P3_1c$ (159) | 6.45 | 4.70 | — | 3.61 | n.d.[a] | 113 |
| β-$C_3N_4$ | $P3$ (143) | 6.35 | 2.46 | — | 3.56 | 250 | 84 |
| β-$C_3N_4$ | $P3$ (143) | 6.40 | 2.40 | — | 3.58 | 451 | 82 |
| β-$C_3N_4$ | $P6_3/m$ (176) | 6.39 | 2.40 | — | 3.60 | n.d. | 113 |
| β-$C_3N_4$ | $P6_3/m$ (176) | 6.44 | 2.47 | — | 3.58 | 427 | 80 |
| c-$C_3N_4$ | $I$-43$d$ (220) | 5.40 | — | — | 3.88 | 496 | 83 |
| pc-$C_3N_4$ | $P$-43$m$ (215) | 3.42 | — | — | 3.82 | n.d. | 113 |
| pc-$C_3N_4$ | $P$-42$m$ (111) | 3.42 | — | — | 3.81 | 448 | 82 |
| g-$C_3N_4$ | $P$-6$m$2 (187) | 4.37 | 6.69 | 90 | 2.35 | n.d. | 113 |
| g-$C_3N_4$ | $P$-6$m$2 (187) | 4.74 | 6.72 | — | 2.33 | n.d. | 82 |

[a] n.d. = not determined.

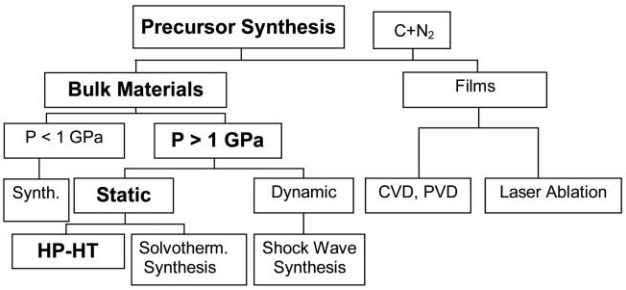


**Fig. 7** The diagram presents an overview of the reported experimental routes to produce $C_3N_4$ phases. The bold route indicates the most promising synthetic pathway, as suggested by several authors.

various starting materials, such as single-source precursors ($C_3N_3(NH_2)_3$, $C_{10}H_{18}N_2O_4S$, $C_2N_2$, $C_6N_4$) or a mixture of compounds between carbon (graphite, $C_{60}$, $CH_4$) and nitrogen ($N_2$, $NH_3$, $Li_3N$, $C_3N_3(NH_2)_3$, $C_6N_7(NCNK)_3$, $C_3N_3Cl_3$, $C_6N_7Cl_3$) sources, have been synthesised.[104–112]

The difficulties faced in the synthesis of carbon nitrides with a $C_3N_4$ stoichiometry are probably related to their low thermodynamic stability with respect to carbon and nitrogen, as indicated by the positive values of their enthalpies of formation.[125] The synthesis at high pressures and temperatures may offer a more promising route to achieving this goal, keeping in view the reported successes in the high-pressure synthesis of other nitrides. An overview of the reported high-pressure experiments with $P > 1$ GPa are listed in Table 2

Predominantly, the products obtained from the high-pressure experiments are amorphous materials, with nitrogen contents much lower than the expected value of 57 at% for $C_3N_4$. In addition, several groups have reported the synthesis of polycrystalline materials consisting of small α-, β- and c-$C_3N_4$ crystallites embedded in an amorphous carbon nitride matrix.

However, none of the theoretically predicted $C_3N_4$ polymorphs have been obtained, or at least reliably characterized in the laboratory, despite statements to the contrary. Despite numerous reports describing the ''successful synthesis'' of different $C_3N_4$ phases, the existence of high density polymorphs of $C_3N_4$ is still a matter of controversy that is discussed within the solid state chemistry and materials science communities.[85–90] Further investigations and detailed analysis are obviously needed to explore, study and determine the existence of crystalline carbon nitride phases and their potentially useful material properties.

Prior to 1999, no examples of silicon or germanium octahedrally-coordinated by nitrogen had been reported in the literature, although such highly coordinated species were well-known to occur among the oxides.[4] In 1999, Kollisch and Schnick reported the synthesis of $Ce_{16}Si_{15}O_6N_{32}$, containing octahedral $SiN_6$ groups.[133] Later in the same year, the nitrides γ-$Si_3N_4$ and γ-$Ge_3N_4$, with a spinel-type structure containing octahedrally-coordinated $SiN_6$ and $GeN_6$ species, were found by means of high-pressure and temperature syntheses in LH-DAC and multi-anvil experiments (Table 3).[55,134,135]

The pioneering synthesis of the cubic nitride γ-$Si_3N_4$ was accomplished by the LH-DAC technique, using elemental Si and $N_2$ as starting materials.[55] In this case, nitrogen adopts

**Table 2** Overview of reported high-pressure experiments at $P > 1$ GPa for the synthesis of $C_3N_4$

| Starting materials | Synthesis conditions | Products $CN_x$ ($x = 1.33$ for $C_3N_4$) | Contamination | Phases | Analysis methods | Ref. |
|---|---|---|---|---|---|---|
| $[C_3N_3(NH_2)_3 + NH_2NH_2]$ | 800 °C, 2.5–3 GPa | $1.14 < x < 1.34$ | O, H | Cryst. | FTIR, XPS, XRD, REM, TEM, ESCA | 96, 114 |
| $[C_3N_3(NH_2)_3 + C_3N_3Cl_3]$, $[C_3N_3(NH_2)_3 + 2C_3N_3Cl_3]$, $C_3N_3(NH_2)Cl_2$ | 500–550 °C, 1.0–1.5 GPa | $1.47 < x < 1.50$ | H, Cl | Partially cryst. | XRD, TEM, EELS, FTIR, NMR | 115 |
| $C_3N_3(NH_2)Cl_2$, $C_3N_3(NH_2)(OH)_2$ | 450–1100 °C, 3.0 GPa | $0.80 < x < 1.46$ | O, H | Cryst. | XRD, FTIR, EA | 116 |
| $C_3N_3(NH_2)_3$ | 400–900 °C, 5.0 GPa | $0.17 < x < 1.91$ | H | Partially cryst. | EA, FTIR, XPS, XRD | 117 |
| C, N, H | 300–400 °C, 6–7 GPa | $x = 0.25$ | O | Cryst. | FTIR, XRD, Raman, | 118–120 |
| $[C_6Cl_6 + NaN_3]$, $[C_6Cl_6 + 3NaN_3]$ | 400–500 °C, 7.7 GPa | $0.70 < x < 1.94$ | O, H | Partially cryst. | HR-TEM, EELS, XRD, FTIR, Raman | 121, 122 |
| $C_3N_3(NH_2)H_2$, $CO(NH)_2$, $NH_4HCO_3$ | 1400 °C, 7 GPa, catal.: Fe, Co, Ni, | $1.09 < x < 1.44$ | n.d. | Partially cryst. | EDX, XRD, REM, | 123 |
| $C_2N_2$ | 550–1000 °C, 10–17 GPa | $0.35 < x < 1.16$ | n.d. | Partially cryst. | XRD | 124 |
| $C_6N_4$ | 2000 °C, 18–42 GPa | $0.56 < x < 0.88$ | H | Amorph.: <18 GPa, Cryst.: >18 GPa | TEM, EELS, WDX, FTIR, Raman | 125 |
| $[C_6N_4 + 2C_3N_{12}]$ | 2500 °C, 119 GPa | n.d. | n.d. | Cryst. | XRD | 126 |
| [Graphite + $N_2$], $[C_{60} + N_2]$, $[C_{amorph.} + N_2]$ | 2000–2500 °C, 30 ± 5 GPa | n.d. | n.d. | Cryst. | XRD | 127 |
| $C_3N_4H_{2.5}$ | 950 °C, 4.8 GPa | $x = 1.1$ | — | t-CN[a] | EELS, SIMS, XRD | 128, 129 |
| $C_3N_3Cl_3$, $C_3N_3H_3$, $C_3N_3(OH)_3$ | 1000–3000 °C, 15–50 GPa (shock-wave) | $x = 1.0$ | H, O, Cl | Cryst. | EA, XRD | 130 |
| a-$C_3N_4$[b] | 500 °C, 8.5 GPa, 1000 s | n.d. | n.d. | Cryst. | XRD, TEM | 131 |
| g-$C_3N_4$[c] | 30 GPa | $x = 1.33$ | — | — | — | 132 |

[a] t- = turbostatic. [b] a- = amorphous. [c] g- = graphitic.

**Table 3** Synthesis details of cubic silicon and germanium nitride $A_3N_4$

| Modification | Starting material | Synthesis conditions | Method | Ref. |
|---|---|---|---|---|
| γ-$Si_3N_4$ | Si + $N_2$ | 15 GPa, 2200 K | LH-DAC | 55 |
| | a-, α-, β-$Si_3N_4$ | 15–30 GPa, ~2800 K | LH-DAC | 136 |
| | α-$Si_3N_4$ | 20 GPa, $T$ = n.d. | LH-DAC | 146 |
| | $Si_2N_2NH$, a-$Si_3N_{3+x}$ | 13–15 GPa, 1873–2073 K | MA | 138 |
| | β-$Si_3N_4$ | 36/>20 GPa, >1300 K | Shock-wave | 154, 155 |
| γ-$Ge_3N_4$ | Ge + $N_2$ | 14–19 GPa, ~2000 K | LH-DAC | 135 |
| | α-$Ge_3N_4$ + β-$Ge_3N_4$ | 14.7 GPa, 1080 K | LH-DAC | 134 |
| | α-$Ge_3N_4$ + β-$Ge_3N_4$ | 12 GPa, 1273–1373 K | MA | 134 |
| | β-$Ge_3N_4$ | 40–46 GPa, 1300–1500 K | Shock-wave | 139 |

simultaneously the role both (i) as the pressure transmitting medium and (ii) as source of one of the reactants.[20] The corresponding cubic spinel phase, γ-$Ge_3N_4$, was synthesized near-simultaneously by two different groups, one using LH-DAC techniques applied to elemental Ge and $N_2$, and the other starting from β-$Ge_3N_4$ in a resistively-heated DAC and a multi-anvil device.[134,135] In later studies, both α- and β-$Si_3N_4$ were shown to transform into the new cubic silicon nitride phase at $P > 15$ GPa and $T > 2200$ K in LH-DAC and multi-anvil experiments, and also by shock-wave treatment.[136–139] Analogously, γ-$Ge_3N_4$ has now been obtained from various mixtures of hexagonal α- and β-polymorphs under DAC, multi-anvil and shock-wave experiments.[134,137]

The structural and chemical characterisation of cubic silicon and germanium nitride, obtained in various LH-DAC, multi-anvil and shock syntheses, has been achieved by Raman spectroscopy,[55,135] X-ray diffraction (XRD),[137] transmission electron microscopy (TEM)[55,135] and energy dispersive X-ray analysis (EDX).[55,134,135] Mechanical properties, such as hardness and elastic moduli, were determined both by *in situ* synchrotron experiments, and by indentation studies of recovered samples.[137–139,155] Optoelectronic properties of the new spinel nitride materials have been investigated by X-ray and optical absorption measurements, as well as predicted by *ab initio* theory.[148,149,161,177]

At the same time as the new polymorphs of $Si_3N_4$ and $Ge_3N_4$ were being reported and investigated, a new $Sn_3N_4$ compound of spinel-type structure was discovered following a synthesis at ambient pressure from chemical precursors. Scotti *et al.* obtained γ-$Sn_3N_4$ by the reaction of $SnI_4$ with $KNH_2$ in liquid ammonia at low temperature.[140] An alternative route to this compound has now been found to involve a solid state metathesis (SSM) reaction at $P$ = 2.5 GPa and $T$ = 623 K (eqn. 2).[141] The presence of $NH_4Cl$ was adjusted to optimize the reaction's temperature and to provide a higher spinel phase yield.

$$3\ SnJ_4 + 4Li_3N \xrightarrow{2.5\ GPa\ /\ 623\ K\ /\ x\ NH_4Cl} Sn_3N_4 + 12\ LiJ \quad (2)$$

The spinel-type structure was described for the first time in 1915 in the form of the type mineral phase $MgAl_2O_4$.[142] In general, spinel compounds are characterized by a composition of $AB_2X_4$, where A and B represent the cations and X the anions. The structure is face-centred cubic with the space group *Fd*-3*m* (no. 227) including $Z$ = 8 formula units. Among the 56 atoms, the 32 X anions lie on the 32*e* site of the structure, while 8 cations are in tetrahedral (*a*) sites and 16 cations are in octahedral (16*c*) sites. Due to the occupation distribution of the two different cations between the tetrahedral and octahedral sites, two classes of spinels have to be considered, denoted as normal spinels and inverse spinels. In a normal spinel ($A(BB)O_4$), the A-cations occupy tetrahedral sites, whereas the B-cations are located at the octahedral site. In inverse spinels ($B(AB)O_4$), the tetrahedral sites are filled fully by B-cations and in the octahedral sites reside the majority B-cations and the minority A-cations.[143] A summary of the structural data determined for silicon, germanium and tin nitride spinels, recovered under ambient pressure and temperature conditions, is presented in Table 4. In γ-$Si_3N_4$, γ-$Ge_3N_4$ and γ-$Sn_3N_4$, nitrogen is four-fold-coordinated by cations (Si, Ge, Sn), while the cations are found in two different environments—in tetrahedral and octahedral coordination to the nitride anions. The unit cell of γ-$Si_3N_4$, with its tetrahedral $SiN_4$ and octahedral $SiN_6$ sites, is depicted in Fig. 8.

**Table 4** Results of the structure refinements of γ-$Si_3N_4$, γ-$Ge_3N_4$ and γ-$Sn_3N_4$

| | γ-$Si_3N_4$ | γ-$Ge_3N_4$ | γ-$Sn_3N_4$ |
|---|---|---|---|
| Space group | | *Fd*-3*m* | |
| $a_0$/Å | 7.8 | 8.3 | 9.03 |
| Formula units, $Z$ | | 8 | |
| Cation positions | Si(1); Ge(1); Sn(1): 8*a*(1/8, 1/8, 1/8) | | |
| | Si(2); Ge(2); Sn(2): 16*d*(1/2, 1/2, 1/2) | | |
| | | N: 32*e*($x$, $x$, $x$) | |
| Anion positions | | $x = 0.25 + \delta$ | |
| | $\delta = 0.00968$ | $\delta = 0.0077$ | $\delta = 0.0095$ |
| Ref. | 55, 138 | 135, 134 | 140 |

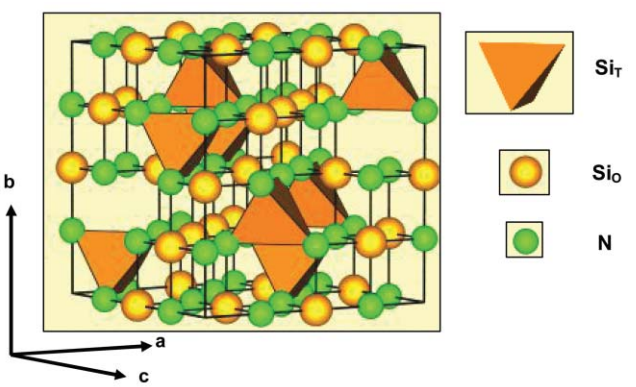


**Fig. 8** Crystal structure of spinel γ-$Si_3N_4$.

**Table 5** Comparison of structural and physical properties of silicon, germanium and tin nitride polymorphs

| Phase | α-$Si_3N_4$ | β-$Si_3N_4$ | γ-$Si_3N_4$ | α-$Ge_3N_4$ | β-$Ge_3N_4$ | γ-$Ge_3N_4$ | γ-$Sn_3N_4$ |
|---|---|---|---|---|---|---|---|
| Structure | *P*31*c* | *P*6$_3$/*m* | *Fd*-3*m* | *P*31*c* | *P*6$_3$/*m* | *Fd*-3*m* | *Fd*-3*m* |
| Density/g cm$^{-3}$ | 3.183[136] | 3.20[136] | 3.93[55] | 5.25[156] | 5.28[156] | 6.36[135] | 6.67 |
| Bulk modulus/GPa | 230[136] | 250[136] | 300[136] | 165[157] | 187[157] | 296[157] 286[153] | 186[153] |
| Hardness ($H_V$)/GPa | 24–45[136] | 14–26[136] | 33[136] 43[153] | — | — | 28 (5)[153] | 28 (5)[153] |
| Band gap/eV | 5.3[158,159] | 5.18[160] | 3.45[161] | 3.18[113] | 3.10[113] 4.03[160] | 2.22[161] | 1.40[161] |
| Thermal expansion coefficient (α)/10$^{-6}$ K$^{-1}$) | 2.4[211] | 3.0[211] | 3.89 (295 K)[162] 3.16 (300 K)[163] | — | — | — | — |

The new spinel nitrides have several potentially useful technological properties that are now being developed for possible applications: they exhibit high hardness and good thermal stability and possess wide direct band gaps (Table 5).[144–153] The synthesis of γ-$Si_3N_4$ spinel using shock-wave methods provides a high throughput route to powdered materials.[154,155]

The formation of ternary spinel nitrides was predicted to occur by analogy with the well-known ternary spinel oxides. On the basis of the successful synthesis of γ-$Si_3N_4$ and γ-$Ge_3N_4$, a new ternary compound was established within the γ-$(Si,Ge)_3N_4$ system.[164,165] Early exploratory experiments were performed in the LH-DAC at pressures about 20 GPa and temperatures up to 2300 K using starting mixtures of α-$Si_3N_4$ and β-$Ge_3N_4$. The reaction products consisted of two co-existing spinels. One had a lattice parameter ($a$ = 7.99–8.01 Å) and revealed a chemical composition of γ-$(Si_{0.05}Ge_{0.95})_3N_4$, very close to that of γ-$Ge_3N_4$. The other spinel phase was much richer in silicon and had a composition of γ-$(Si_{0.59}Ge_{0.41})_3N_4$. Due to the relative intensities of the X-ray diffraction patterns, the authors judged that the new phase was a normal spinel, with $Si^{4+}$ occupying the octahedral sites and $Ge^{4+}$ located in the tetrahedral sites.[164]

Dong *et al.* investigated the thermodynamic stability of solid solutions and intermediate compounds within the ternary spinel nitride system $Si_3N_4$–$Ge_3N_4$.[166] The ternary normal spinel, $GeSi_2N_4$, was predicted to form a stable phase within the system. It was further predicted to have a Vickers hardness of 28 GPa and a direct wide-band gap. More recently, Soignard *et al.* re-investigated the $Si_3N_4$–$Ge_3N_4$ spinel system using multi-anvil high-pressure and temperature synthesis methods, and reported the preparation of continuous solid solutions at $P$ = 23 GPa and $T > 2000$ °C. An unexpected result of these studies was finding that the nominally larger cation $Ge^{4+}$ occupied the tetrahedral sites within these ternary spinel nitride structures and the "smaller" $Si^{4+}$ cation occupied the "larger" octahedral sites. The result was rationalised by considering the bond valency and site preference requirements around the anion $N^{3-}$. These considerations provided a new way of understanding site occupancies within spinel structures.[164,166,241]

The first ternary crystalline compounds in the SiCN system, namely $SiC_2N_4$ and $Si_2CN_4$, were discovered in 1997 under ambient pressure.[167] In theoretical publications, such crystalline SiCN compositions had been proposed as potentially new precursors for superhard ceramics, as their composition is located directly on the tie line between the hypothetical $C_3N_4$ and $Si_3N_4$ in the isothermal section of the ternary SiCN phase diagram.[167,168] Very recently, Kroll calculated a linear interpolation (*i.e.*, using Vegards' law) between $C_3N_4$ and $Si_3N_4$, pointing out a possibility of the high-pressure synthesis (~35 GPa) of a $Si_2CN_4$ phase with the willemite-II structure.[169] Lowther *et al.* dedicated two theoretical papers to the computational design of new advanced materials in the SiCN system.[170,171] In one publication, the potentially superhard material β-$SiC_2N_4$ was compared with hypothetical β-$C_3N_4$ by replacing two C atoms with Si in the 14-atom unit cell of β-$C_3N_4$.[170] The relaxation of Si atoms leads to a hexagonal *P*2/*m* structure. The calculated bulk modulus ($B$) of β-$SiC_2N_4$ (330 GPa) is about ⅔ that of β-$C_3N_4$ (432 GPa) and shows that the origin of the high bulk modulus is related to strong C–N bonds. The lower limit of conversion pressure in order to overcome the energy barrier between the experimentally synthesized cubic form of $SiC_2N_4$ and the hexagonal form of β-$SiC_2N_4$ was predicted to lie between 6–12 GPa. The second report examined several structural forms of Si-rich $Si_2CN_4$ and their properties, and a possible spinel-structured phase was investigated. The predicted bulk modulus was large (344 GPa). However, we now recognize from further theoretical calculations that the inclusion of C into β-$Si_3N_4$ network structures dominated by Si should cause such great elastic stress that no new β-$Si_2CN_4$ phases would be energetically favored.[172]

The various theoretical predictions are tested, supported and complemented by high-pressure and temperature studies, including synthesis and recovery experiments. In the case of SiCN phases, Solozhenko *et al.* (2004) have studied $Si_2CN_4$ up to 8 GPa and reported its equation of state using EDX diffraction with synchrotron radiation.[173] The compressional behavior is distinctly anisotropic due to the particular solid state structure of silicon(carbodimide)nitride, $Si_2CN_4$, which is significantly more compressible in the b-direction, determined by the flexibility of Si–N=C bond angles in the b-direction *vs.* the rigid Si–N–Si bond angles in the a- and c-directions.

### 3.2 Binary and ternary transition group element nitrides

A logical extension of the work described above on the spinel-nitrides of group 14 elements, γ-$M_3N_4$ (M = Si, Ge and Sn), were experiments on the synthesis of high-pressure nitrides of group 4 elements (Ti, Zr and Hf) having, similar to Si, Ge and Sn, four valence electrons. Even though Ti, Zr and Hf exhibit the maximal oxidation number of +4 in many of their compounds, including the oxides, special efforts are required

in order to attain an oxidation state higher than +3 in the compounds with nitrogen. Prior to high-pressure synthesis experiments, the existence of a bulk stoichiometric nitride with a cation valence of +4 had been confirmed only for $Zr_3N_4$.[174–176] Following the discovery of spinel nitrides of the group 14 elements, the stability and properties of corresponding hypothetical dense nitrides of other elements of +4 valency were considered theoretically.[177–179] The predicted structure and physical properties of three forms of $Zr_3N_4$, namely γ-$Zr_3N_4$, orthorhombic-$Zr_3N_4$[174–176] and an ordered defect model with the rock salt structure, $Zr_3\square N_4$, were calculated and compared.[180] It was predicted that $Zr_3\square N_4$ would have the lowest energy at ambient pressure. In contrast to these predictions, a previously unknown family of high-pressure nitrides of the group 4 elements, having the stoichiometry $A_3N_4$ (A = Zr and Hf) and a cubic $Th_3P_4$-type structure, was synthesized experimentally using LH-DAC techniques.[77] The research has been extended further to the synthesis of novel nitrides of other transition metals such as molybdenum,[181] platinum and iridium.[182,183]

In the first high-pressure experiments on the synthesis of stoichiometric $A_3N_4$, chemical reactions of zirconium and hafnium metals, and of their mono-nitrides (δ-AN), with nitrogen were ignited in a LH-DAC at 16–18 GPa by heating with a Nd:YAG laser to 2500–3000 K.[77] The reaction products were the stoichiometric nitrides $Zr_3N_4$ and $Hf_3N_4$, having cubic $Th_3P_4$-type structures (Fig. 9A), denoted hereafter as c-$A_3N_4$.[77] The stoichiometry and structure were verified by XRD and EDX measurements. This work presented the first evidence for the existence of a new bulk hafnium nitride compound of stoichiometry $Hf_3N_4$. In the $Th_3P_4$-type structure, the coordination number of the anions is six (Fig. 9C) and the cations is eight (Fig. 9B)—well above that in the spinel or NaCl-type structure or in the NaCl-type structure of the mono-nitrides δ-AN. Moreover, novel c-$A_3N_4$ (A = Zr and Hf) are the first binary nitrides to have such a high cation coordination number. The cubic lattice parameter of c-$Zr_3N_4$, with $a_0$ = 6.740(6) Å, was found to be larger than that of c-$Hf_3N_4$, with $a_0$ = 6.701(6) Å. This finding is in line with the general trend that lattice parameters and/or volumes of binary hafnium compounds (nitrides, oxides, phosphides, fluorides, *etc.*) are smaller than those of the corresponding zirconium compounds. The density of c-$Zr_3N_4$ was analyzed to be $\rho$ = 7.159 g cm$^{-3}$, which exceeds that of the previously reported orthorhombic-$Zr_3N_4$ by about 13%.

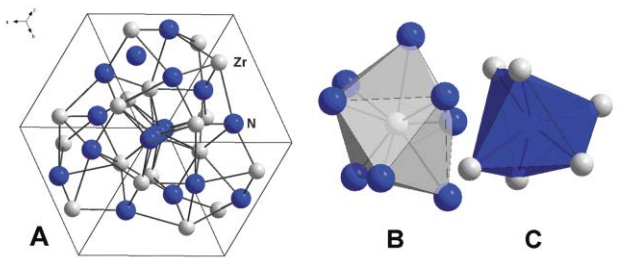


**Fig. 9** Ball-and-stick model of c-$Zr_3N_4$, having a $Th_3P_4$-type structure (A). In this structure, cations and anions are eight- and six-fold-coordinated, respectively. The coordination polyhedron of Zr cations is an irregular octaverticon (B). The coordination polyhedron of N anions can be considered as a distorted octahedron (C).

For the synthesis of macroscopic amounts of c-$A_3N_4$ at high pressures and temperatures in large volume, high-pressure devices, large quantities of starting materials with a nitrogen-to-metal ratio $N : A > 4 : 3$ are required. After extended research, suitable starting materials were prepared. In particular, nanocrystalline powders of $Zr_3N_4$ and of nitrogen rich $Hf_3N_4$ were synthesised *via* a simple process of the ammonolysis of metal dialkylamides, *i.e.* $Zr(NEt_2)_4$ and $Hf(NEt_2)_4$, at temperatures below 700 °C.[184] The obtained nitrides were found to have a rhombohedrally-distorted NaCl-type structure, which was previously reported only for nitrogen rich films of these compounds.[185] Very recently, nanocrystalline $Zr_3N_4$ was used as a starting material in the successful synthesis of c-$Zr_3N_4$ in a multi-anvil high-pressure device.[186] The obtained samples were used to determine the elasto-mechanical properties and thermal stability of c-$Zr_3N_4$.

The ability of the LH-DAC to achieve very high temperatures at high pressures was used recently to transform the mono-nitride of molybdenum (MoN) into the structure with ordered positions of anions in the crystal lattice.[181] At ambient pressure, the solid state synthesis methods (*e.g.* ammonolysis of $MoCl_5$ at high-temperature) result in a disordered material, with a hexagonal structure described by the *P*-6*m*2 space group, similar to that of WC. Laser heating of this material in a DAC to about 2800 K at 5.6 GPa led to a transformation into an ordered material of excellent crystallinity, whose hexagonal structure is described by another space group $P6_3mc$.[181]

Very recently, the discovery of the first noble metal nitride, namely platinum nitride, was reported. It is not surprising that this compound was synthesized from elements in a LH-DAC at pressures in excess of 45 GPa.[182] The material obtained was found to be quenchable under ambient conditions and was initially believed to be a mono-nitride with a minor deficit of nitrogen, $PtN_{1-x}$ ($x < 0.05$). The structure was suggested to be cubic and related to that of zinc blende. However, the extra peaks in its Raman spectrum and the XRD pattern of the reaction product could not be explained by this structure. A potential shortcoming of this report was the lack of information on the method used to load the nitrogen into the LH-DAC. The bulk modulus of this cubic platinum nitride was measured as 354–372 GPa, which is similar to that of cubic BN. However, subsequent theoretical considerations indicated that the suggested structure and, most probably, the composition of the synthesized material had to be revised. The first argument for the revision was the 50% lower bulk modulus of PtN with the zinc blende structure, independent of the method used in these first principles calculations.[187–192] Furthermore, the zinc blende structure of PtN was found to be mechanically unstable, since the value of the elastic stiffness constant $C_{11}$ was found to be lower than that of $C_{12}$. This required spontaneous distortion of the cubic lattice to a tetragonal one.[191,192] It was suggested that all tetrahedral interstitial sites of the metal sub-lattice of the cubic platinum nitride, not a half, as in the zinc blende structure, could be occupied by nitrogen anions. The stoichiometry of the compound would be then $PtN_2$ and its structure of the fluorite type.[192] For the latter material, the bulk modulus was calculated to be about

 

290 GPa, which is still 22% below the experimental value.[191,192] As a consequence of these theoretical considerations, the first author of the original experimental publication revised, after further measurements, the stoichiometry of the platinum nitride to $PtN_2$ but did not suggest any solution for the structure.[193] In very recent work on the high-pressure synthesis of platinum and iridium nitrides, both PtN (with the zinc blende structure) and $PtN_2$ (with the fluorite-type structure) were calculated to be highly unstable at both high and ambient pressures.[183] Due to this finding, the authors re-examined the composition and structure of the material they obtained at about 50 GPa and 2000 K in the reaction of platinum and molecular nitrogen, loaded cryogenically. They also reported to have synthesized an iridium nitride under similar pressure and temperature conditions. Examination of samples using EDX and XPS revealed that the reactions were not complete and that nitrogen was not homogeneously distributed in the reaction products. From a comparison of the shifts in binding energies of the observed elements, the most probable composition of both nitrides was estimated to be $PtN_2$ and $IrN_2$. Oxygen peaks were also detected in the EDX and XPS spectra, but the authors attributed them to adsorbed water.[183] In this work, another cubic structure, related to that of pyrite ($FeS_2$), was reported to better match the observed Raman spectra and preliminary X-ray powder diffraction pattern of platinum nitride. This structure solution was further supported by *ab initio* calculations. In contrast, the structure of the obtained iridium nitride was found to have much lower symmetry than that of cubic.

Despite the obvious uncertainties in the stoichiometries and structures, the discovery of noble metal nitrides demonstrates impressively that the application of high pressures and temperatures is one of the most promising ways to explore new advanced materials that are not accessible at ambient pressure. Following this idea, a systematic study on the formation and crystal structure of 3*d*-transition metal (Ti–Cu) nitrides was performed at nitrogen pressures up to 10 GPa and temperatures up to 1800 K.[194,195] The synthesis was performed, once again, in a LH-DAC *via* direct nitriding of elemental metals. Since the applied pressures were relatively low, only the phases and compounds reported earlier were found.

Examination of the properties and possible applications of high-pressure transition metal nitrides is still in its infancy, mostly due to the absence of macroscopic amounts of these materials. As already mentioned above, for nitrides of the group 4 elements having the $Th_3P_4$-type structure (c-$A_3N_4$), this obstacle is now eliminated. Moreover, first reports have appeared on the outstanding mechanical properties of the high-pressure transition metal nitrides, demonstrating their potential industrial applicability.

In the original report on the stoichiometric nitrides of zirconium(IV) and hafnium(IV), c-$A_3N_4$, where A = Zr or Hf, large bulk moduli of around 250 GPa were derived from preliminary compression measurements and high hardnesses were suggested.[77] Subsequent theoretical calculations have not only confirmed the structures but also large bulk moduli for both compounds.[196,197] The shear moduli were predicted to be around 150 GPa, similar to the lower limit value measured for the cubic silicon nitride of spinel structure, $\gamma$-$Si_3N_4$.[147] Such shear moduli could be considered moderate compared to other superhard materials such as diamond or cubic boron nitride. Furthermore, these two nitrides were considered as the first members of a large group of high-pressure transition metal nitrides with interesting functional, magnetic or superconducting properties.[77] Theoretical calculations on c-$A_3N_4$ have also shown that they are semiconductors with small-band gaps.[196,197] In a very recent detailed study of the compression behavior of c-$Hf_3N_4$ at room temperature to about 44 GPa, its bulk modulus, $B_o$, was determined to be 227(7) GPa and the first pressure derivative, $B_o'$, to be 5.3(6).[198] Assuming the first pressure derivative to be $B_o' = 4$, the bulk modulus was derived in the same work as 241(2) GPa. Another author's group has presented an outstanding observation that, using a modified filtered cathodic arc method, c-$Zr_3N_4$ can be deposited on carbides as a thin film (about 1 μm in thickness) with good adhesion.[199] Moreover, the films of c-$Zr_3N_4$ were shown to have an extraordinary wear resistance by the machining of low carbon steel. The new hard material "dramatically outperforms" uncoated carbide tools, as well as those coated with traditional δ-TiN; the wear resistances differ by about one order of magnitude.[199]

The first work on the synthesis and characterization of a platinum nitride attracted attention by its finding that the bulk modulus of this noble metal nitride, 372 GPa, was similar to that of cubic BN.[182] This result was supported by the later work of Crowhurst and colleagues, who reported a $B_o$ value in the range 350–410 GPa.[183] Independent of the uncertainties over the composition and structure of this platinum compound (considered above), this exciting result gave the hope that other noble metal nitrides with outstanding physical properties would be discovered. The hope is supported by reports on the synthesis of iridium and osmium nitrides at high pressures.[183,200,201] For iridium nitride, a bulk modulus value similar to that of platinum nitride was suggested.[183] However, it has to be investigated in more detail if the quite large experimental value of $B_o$ reported for platinum nitride could be biased by the suggested structure.

## 4. Oxonitrides

A useful strategy in new materials synthesis is to integrate and optimize the properties of end-member components through the formation of compounds containing mixed cation or anion species. This has led to the development of new families of oxynitride materials that can have structures and properties related to those of their parent oxides and nitrides, but that can also be quite different. High-pressure syntheses and studies on oxynitride compounds are only now beginning to lead to entirely new classes of materials having interesting physical properties.

In general, bonding among solid oxides is more ionic than in the corresponding nitrides. Main group oxide compounds are usually insulators, whereas nitrides are often wide-gap semiconductors. Among the transition metal oxides, a wide range of oxidation states are encountered, usually including the maximum oxidation number for each metal. The metal atoms in the corresponding nitrides generally possess lower oxidation states, and the compounds are usually best described

as structures containing interstitial N atoms, with the bonding dominated by metal–metal interactions.[202–204] The same is true among the corresponding carbides (*e.g.*, TiN, WC). The metallic nitrides are often superconductors, and can achieve high values of $T_c$ (*e.g.*, up to 13–17 K for cubic NbN and ordered hexagonal MoN).[203–210] The metal nitrides and carbides possess a high cohesive energy, which makes them highly refractory. They are very high hardness materials, developed for cutting and grinding applications, and as scratch-resistant coatings (TiN, WC, *etc.*).[202,203] The nitrides of main group elements provide important ceramics ($Si_3N_4$, AlN).[211,212] They also give rise to wide-gap semiconductors (*e.g.*, GaN, InN), in which direct band gaps can lead to important applications in light-emitting diodes and solid state lasers.[15,16] Transition metal oxides tend to be highly refractory due to their ionic bonding, but they are generally less refractory than their corresponding nitrides and also have lower hardness (*e.g.*, $TiO_2$ and $ZrO_2$ *vs.* ZrN and TiN). However, some highly-coordinated transition metal oxide structures synthesized under high-pressure conditions (*e.g.*, $RuO_2$) are predicted to lead to very incompressible and high hardness materials,[213–215] as are new metal nitride compounds obtained at high-pressure ($Zr_3N_4$, $PtN_x$).[77,182,183] High-pressure syntheses have also resulted in novel high density oxides and nitrides of main group elements ($SiO_2$, $Si_3N_4$, $P_3N_5$).[55,216–218] The formation of oxynitrides permits tuning of the bonding and electronic properties. There has been recent progress in the synthesis and studies of new families of oxynitride materials at high-pressure.

In the 1970s, these compounds were first proposed as a new class of ceramics in the $SiO_2$–$Al_2O_3$–$Si_3N_4$–AlN system. They were, in part, designed to improve the oxidation resistance and high-temperature mechanical properties of $Si_3N_4$, which is a well-known refractory ceramic used extensively for engine parts and gas turbines, and in cutting and grinding tools.[219–228] A series of solid solutions based on the β-$Si_3N_4$ structure has the general composition $Si_{3-x}Al_xO_xN_{4-x}$ for $x < 2.1$; these are termed the " β′-sialons" (SiAlONs).[229,221,222,230] They also have certain structural features in common with the ceramic phase mullite, which exists over a compositional range within the $SiO_2$–$Al_2O_3$ system. The β′-sialon structures contain polymerised $Si(O,N)_4$ and $AlN_4$ tetrahedra, and $AlO_x$ groups. Other families of SiAlONs include yttrium-containing phases like $YSiO_2N$, with a chain structure like that of wollastonite ($CaSiO_3$), $Y_2Si_3O_3N_4$ melilite, and $Y_5(SiO_4)_3N$, which is isostructural with apatite, $Ca_5(PO_4)_3OH$.[231,232] These phases can be structurally correlated with the α-$Si_3N_4$ polymorph and provide useful hosts for luminescent ions such as $Tb^{3+}$. SiAlON-based compounds like $Li_2SiAlO_3N$ have a "stuffed" cristobalite structure, in which the fully polymerised framework is formed by corner-shared $(Si,Al)(O,N)_4$ tetrahedra. SiAlON glasses have been reported and studied.[233] These amorphous phases form an intergranular cement in the high-temperature sintering of oxynitride ceramics and provide important ceramics in their own right.[226,234] A series of layered $AlO_xN_y$ compounds, extending into the SiAlON system from the $Al_2O_3$–AlN binary, is also well-known.[235,228] These materials possess layered structures derived from the close-packed arrangement of anions and cations found in wurtzite-structured AlN (*hcp*) or its sphalerite-structured equivalent (*ccp*), arranged in various stacking sequences. Metastable polymorphs of $Al_2O_3$ are known to form "defective" spinel structures based on a *ccp* array of $O^{2-}$ ions, with tetrahedrally- and octahedrally-coordinated $Al^{3+}$ cations that can contain vacancies on both cation and anion sites. Oxynitride spinel structures are formed close to the composition $Al_3O_3N$.

Dense oxynitride and nitride ceramics are usually processed as polycrystalline materials *via* "hot-pressing" methods in high-pressure gas environments at $T \sim 1500$–$1800$ °C and at a few atmospheres pressure. These pressurization conditions are ideal to achieve the synthesis and sintering of high density polycrystalline materials, but are not sufficient to effect structural phase transitions into new high-pressure polymorphs. Recently, high-pressure experimental techniques at $P > 10$ GPa and extending into the megabar range ($P > 100$ GPa) have been applied to study the synthesis and solid state chemistry of oxide and nitride compounds. These experiments, combined with theoretical predictions, have resulted in the discovery of several new high density polymorphs, including phases in the SiAlON and related systems. These techniques are now being applied to investigate the high-pressure and temperature phase relations, and solid state chemistry, of oxynitride materials.

The oxynitride spinel samples were determined to have a Vickers hardness, $V_H$, of ~ 27.5 GPa, greater than that of γ-$Si_3N_4$, and the fracture toughness (4.6 MPa $m^{1/2}$) was found to be comparable with the upper range of values recorded for the tetrahedrally-coordinated SiAlONs (3–4.5 MPa $m^{1/2}$).[236]

Within the system Al–O–N, spinel-structured compounds occur close to the ideal composition $Al_3O_3N$. Corresponding $Ga_xO_yN_z$ spinels could be of interest as selective reduction catalysts, as gas sensors, and as electron emitters, magnetic memory materials or wide-gap semiconductors for optoelectronic applications. Gallium oxynitride, $Ga_3O_3N$, was predicted theoretically to form a new spinel-structured compound within the $Ga_2O_3$–GaN system.[237] There were early experimental reports of a cubic gallium oxynitride phase with a composition close to $Ga_{2.8}O_{3.5}N_{0.5}$ that formed metastably during GaN thin film synthesis from chemical precursors.[238,239] Formation of a new spinel-structured compound with a composition close to $Ga_3O_3N$ has now been reported as a result of high-pressure and temperature syntheses.[240,241] The experiments used a combination of LH-DAC and multi-anvil synthesis techniques to establish the formation of spinel-structured $Ga_xO_yN_z$ materials from $Ga_2O_3$ and GaN mixtures, or using organometallic precursors. The materials were characterised both *in situ* and following recovery using a variety of methods, including electron microprobe analysis to determine the composition, electron and X-ray diffraction followed by Rietveld analysis to determine the structure, and Raman spectroscopy combined with *ab initio* calculations to determine the lattice dynamics and the influence of O/N disorder. Both sets of high-pressure syntheses resulted in a new spinel-structured material that was slightly O-rich and N-deficient compared with the ideal $Ga_3O_3N$ phase, with a chemical composition close to $Ga_{2.8}N_{0.64}O_{3.24}$. The compound was also shown to contain vacancies at the octahedrally-coordinated $Ga^{3+}$ sites.

 

The silicon oxynitride compound $Si_2N_2O$ has a structure based on $SiO_3N$ tetrahedra. It is found as a natural mineral (sinoite) within meteorite samples and is also present as an interface phase in polycrystalline oxide–nitride ceramic composites. An early study of the compressional behavior of $Si_2N_2O$ and $Ge_2N_2O$ was carried out by Catz and Jorgensen.[242] The oxynitrides exhibited a compressibility that was intermediate between those of the nitrides and corresponding oxides. Kroll and Milko recently evaluated the possibility of synthesising new $Si_2N_2O$ materials under high-pressure and temperature conditions.[243] Sekine *et al.* studied the recovered products from shock-wave treatment of sinoite powders to 28–64 GPa.[244] Above 34 GPa, partial amorphisation of the silicon oxynitride was observed, and the process was essentially complete by 41 GPa. This indicates that some of the high density phases predicted by Kroll and Milko might be accessible *via* high-pressure and temperature synthesis. Aluminum oxynitride (AlON) has now been investigated at high-pressure using a shock-wave treatment to 180 GPa.[245] The Hugoniot data indicate that a possible phase transition into a $CaTi_2O_4$-type structure may occur at above $\sim$130 GPa.

Phosphorous nitride-hydrides and related oxynitride compounds are generally known as ''phosphams'' and exhibit useful flame retardant properties. They have been proposed as high dielectric insulating substrates for electronics applications.[246–249] Phosphorus pentoxide ($P_2O_5$) is a soft deliquescent covalently-bonded solid used as a desiccant. $P_3N_5$ is a well-known compound[250] that has, however, only recently been crystallised for structure determination.[251,252] Recent high-pressure studies, combined with *ab initio* calculations, have revealed the existence of new high density forms of this material containing unusual highly-coordinated $PN_5$ and $PN_6$ groups.[216–218] These are expected to possess high hardness along with lower chemical reactivity. Various phosphorus oxynitrides and isoelectronic nitride-imide compounds (*i.e.*, $PN_x(NH)_y$) are known from metastable synthetic routes at ambient pressure.[253]

The oxynitride PON is isoelectronic with $SiO_2$, and the compound synthesised under ambient conditions is isostructural with a tetragonally-distorted version of the silica polymorph cristobalite (*I*-42*d* symmetry).[254] Various polymorphs of phosphorus oxynitride have been investigated *in situ* at high-pressure and ambient temperature, and also *via* high-pressure and temperature synthesis methods. PON first exhibits a transformation into a moganite-structured phase at high-pressure and high-temperature (2.5–4.5 GPa, 850–1010 °C), corresponding to a cell-doubled variation of the $SiO_2$-quartz structure containing right- and left-handed spiral chains of $P(O_2N_2)$ tetrahedra: this phase can be quenched metastably to ambient pressure and temperature,[255–258] At higher pressure, a quartz-structured polymorph is obtained that can also be recovered under ambient conditions.[257,259] The PON polymorphs are observed to be significantly less compressible than their corresponding $SiO_2$ phases.[260–264] The cristobalite-structured material exhibits a remarkable resistance to structural change upon densification: it can be compressed metastably up to at least 70 GPa.[257,260,261,264] However, the quartz polymorph of PON undergoes pressure-induced amorphisation above 30 GPa.[259] Similar differences in amorphisation behavior are recorded between the quartz and cristobalite polymorphs of $SiO_2$. At pressures above approximately 9 GPa, the rutile-structured $SiO_2$ phase stishovite, containing octahedrally-coordinated $SiO_6$ groups, becomes stable. However, there has been no report to date of a similar highly-coordinated PON compound obtained by high-pressure and temperature synthesis.[257] The analogous phospham compound $HPN_2$ (*i.e.*, PN(NH)) likewise has a tetragonally-distorted cristobalite structure[265] and has been studied *in situ* by X-ray diffraction and vibrational spectroscopy techniques to a very high-pressure at ambient temperature. Here the structure demonstrably remains metastable to $P$ = 80 GPa, well above the stability limits of any tetrahedrally-coordinated $SiO_2$ polymorphs.[260]

Phosphorus oxynitride glassy compounds are known.[266,267] High-pressure synthesis methods were used to prepare the first pure nitride glasses within the system $Li_3N$–$Ca_3N_2$–$P_3N_5$.[268,269] In this case, the high containment pressure was used to maintain a high chemical activity of nitrogen above the melt and not to study densification of the glass. From previous studies of coordination increases and viscosity changes among silicate and aluminosilicate liquid glasses and liquids,[270–272] it is likely that new structural principles and properties of nitride and oxynitride glasses will result from high-pressure investigations of these materials.

Many transition metal oxynitrides, especially compounds of the 4d and 5d metals such as Ta, Hf and Zr, are now known to have electronic and mechanical properties that can be intermediate to those of their oxide and nitride components, or can have quite different behavior to the end-members.[273] The introduction of oxygen into nitrides, such as $Ta_3N_5$, that are developed as pigments can permit adjustment of their colour.[274] A wide variety of complex alkali- or alkaline-earth and Si-bearing oxynitride compounds with transition metals and lanthanides have now been synthesized.[275–278] Nitrides and oxynitrides of 2nd- and 3rd-row transition metals, lanthanides and actinides that can possess high oxidation states have given rise to new families of densely-packed compounds, for example with rock salt and perovskite structures.[279–284] These structures might be accessed among new oxynitride materials in high-pressure synthesis experiments.

The ceramic phase $ZrO_2$ is a well-known solid electrolyte that is used as an $O^{2-}$ sensor in high-temperature applications. The compound has a cubic fluorite structure under ambient pressure and temperature conditions. It readily undergoes transformation into a tetragonal polymorph under the influence of non-isotropic stress, such as that induced by a propagating crack system, and it has become important as a fracture toughening agent in ceramic composites. $HfO_2$ has a similar structure and properties. Zr and Hf nitrides are known to occur with a defective rock salt structure ($Zr_xN$) like the corresponding titanium nitride materials, which have applications as high hardness coatings. An orthorhombic structure of $Zr_3N_4$, which formally contains $Zr^{4+}$ ions in octahedral and trigonal-prismatic coordination, has also been prepared.[285] At high-pressure, $Zr_3N_4$ and $Hf_3N_4$ form $Th_3P_4$-type structured phases, with the transition metals being eight-fold coordinated (see Section 3.2).[77] These materials are highly incompressible and could possess high hardness values. Zr and Hf oxynitride

phases have also been prepared at ambient pressure, and crystalline and amorphous oxynitrides within the system Zr–Si–O–N have also been prepared *via* "carbonitridation" reactions (*i.e.*, the reduction of oxides by C with simultaneous nitridation). These materials could lead to new families of refractory ceramics, and they represent useful targets for future high-pressure and temperature syntheses.

## 5. Nitride-diazenides

The binary systems of alkaline earth metal–nitrogen and their intermediate compounds have been the subject of numerous discussions for many years. Recently, a reactive gas high-pressure synthesis led to single phase nitride-diazenides products for the first time. Using this method, it was possible to synthesize nitrogen rich compounds free of impurities such as hydrogen, carbon and oxygen.[286–289] The most important variable with regard to phase formation and composition is the reactive gas pressure. The formation of the different phases can be described in terms of reversible redox-intercalation processes. Starting from $Sr_2N$ as the host structure, diazenide dumbbells are inserted, accompanied by simultaneous oxidation of strontium to $Sr^{2+}$. The stepwise intercalation proceeds with increasing reaction pressure until the final state, of chemical composition $SrN_2$, is reached.

The nitrogen pressure reaction series $Sr_2N$–$Sr_4N_3$–SrN–$SrN_2$ were synthesized as single-phase products in autoclaves by reaction of the freshly prepared sub-nitride $Sr_2N$ with molecular nitrogen at 920 K in the pressure region 9–5500 bar. A sketch of the reaction and decomposition conditions is shown in Fig. 10.[286,287]

The crystal structures of these strontium nitride-diazenides were determined by a combination of X-ray and neutron diffraction experiments on microcrystalline powders at ambient conditions (Fig. 11). Summing up the results concerning the physical properties in a very condensed manner, the binary system strontium–nitrogen undergoes a stepwise reversible change from metallic to semiconductor properties by variation of the nitrogen reaction pressure.

The evident structural relationship between the mentioned binary compounds makes it reasonable to suppose a reaction path leading to the formation of nitride-diazenides *via*

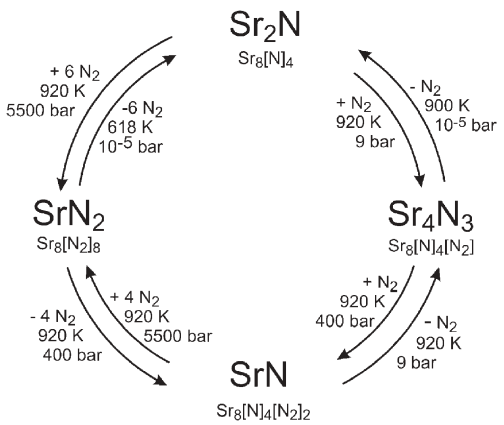


**Fig. 10** Schematic representation of the reversible strontium–nitrogen pressure series.

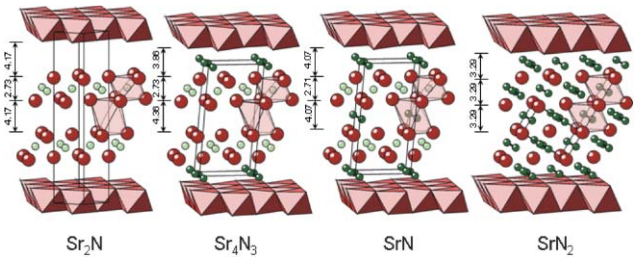


**Fig. 11** The crystal structures of $Sr_2N$, $Sr_4N_3$, SrN and $SrN_2$. The top and bottom boundaries of the figures are represented by layers of $Sr_{6/3}$ octahedra (polyhedral representation) centred by $[N^{3-}]$ ($Sr_2N$, $Sr_4N_3$ and SrN) and $[N_2^{2-}]$ ($SrN_2$), respectively. Ball-and-stick representations are used between the polyhedral layers: $Sr^{2+}$= red, $[N^{3-}]$ = light green, $[N_2^{2-}]$ = dark green. Transparent octahedra allow a better visual orientation.

intercalation steps that preserves the topochemical host–guest relationship. Starting from $Sr_2N$, which crystallizes in a $CdCl_2$-type structure, half of the unoccupied octahedral holes of every second layer become filled with $[N_2^{2-}]$ in the first intercalation step ($Sr_4N_3$ = $Sr_8[N^{3-}]_4[N_2^{2-}]$). With increasing nitrogen pressure, SrN ($Sr_4[N^{3-}]_2[N_2^{2-}]$) is formed by filling up half of the octahedral holes of the hitherto empty layers. In the final step, in $SrN_2$ ($Sr[N_2^{2-}]$), the remaining empty octahedral holes are filled by $[N_2^{2-}]$ and, simultaneously, the $[N^{3-}]$ ions within the strontium arrangement are replaced by diazenide ions (reaction of $N_2$ with $N^{3-}$).

Besides investigating the crystal structures, a definite knowledge of the chemical composition of a compound, as well as any impurities present in the powder material, is essential for the interpretation of its chemical and physical properties. In addition to the overall quantitative determination of elements in materials, the field of element speciation is of importance in order to gain a valuable insight into the different species of elements that may be present in a single compound. Therefore, application of the carrier gas hot extraction (CGHE) method, including speciation of nitrogen, was focused on the binary alkaline earth metal–nitrogen compounds. A precise and accurate analysis of the nitrogen content succeeded after developing a method that allowed controlled and variable heating. By means of this method, it is possible to verify not only the existence of, but also to quantify different nitrogen species.[290] Moreover, the strength of detection of the CGHE method can lead to the detection of formerly unknown compounds. For example, in the course of our studies on binary strontium nitrogen compounds, it turned out that even $Sr_2N$ synthesized at ambient pressure often contains significant portions of an additional diazenide phase that was not detected by means of X-ray and spectroscopic investigations, whereas the technique of controlled temperature heating shows a small but reproducible peak at low temperature for the reaction products, indicating two different nitrogen species being present in the sample. The exact analysis of the analytical results led to the previously overlooked compound $Sr_4N_3$, which is already found as an impurity phase in varying but small amounts during the synthesis of $Sr_2N$ at ambient pressure.[287]

 

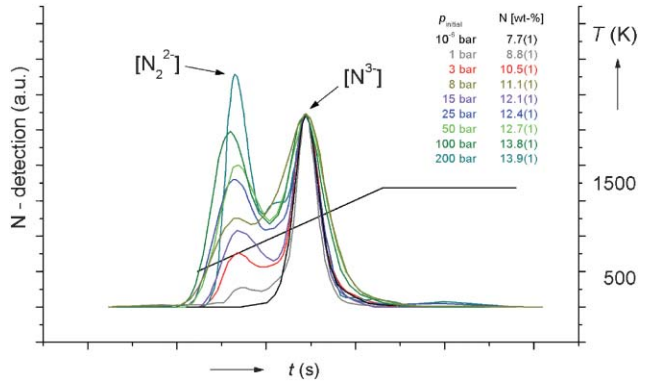


**Fig. 12** Results of the CGHE studies on $Sr_2N$, $Sr_4N_3$ and SrN: Correlation of detected signal and heating rate with increasing reaction pressure, scaled to the peak indicating the $[N^{3-}]$ content. $SrN_2$ (showing a single peak only, indicating the $[N_2^{2-}]$ species) is omitted for clarity.

Fig. 12 shows that, under well adapted conditions, separate peaks become visible that can be attributed to different species of nitrogen ($[N_2^{2-}]$ and $[N^{3-}]$). For example, the binary subnitride exclusively contains one nitrogen species, $[N^{3-}]$, indicated by a single peak, as expected from its chemical formula. The nitride nitrogen in $Sr_2N$ is released at a higher temperature in comparison to the $[N_2^{2-}]$ species. In addition, the CGHE method reveals that the impurities (H, C, O) were below the detection limits. The analytical results show that the CGHE technique represents a powerful tool for the chemical characterisation of nitrogen compounds.

The diazenide species ($d_{N=N}$ = 1.22 Å) were characterized by spectroscopic methods. All attempts to record Raman spectra failed, even though different laser frequencies and preparation conditions were used. Finally, vibrational modes could be detected by inelastic neutron scattering experiments using the spectrometers TOSCA and MARI at ISIS, and showed that the diazenide ions lie trapped within the cage of the strontium atoms.[291] The N=N stretch of the diazenide ions are assigned at 1380 (SrN) and 1307 ($SrN_2$) $cm^{-1}$, respectively.

Additional studies in the Ba–N system clearly show that, starting from $Ba_2N$, an insertion of nitrogen in the host structure succeeds, in analogy to the strontium system, by increasing the $N_2$ reaction pressure; however, the pressure regions leading to pure intercalated phases are significantly lowered and smaller. Thus, the pure diazenide $BaN_2$ is already obtained at 400 bar $N_2$ reaction pressure, and reaction pressures in an even lower range reveal the existence of $Ba_4N_3$ and BaN.[288,289] The nitrogen content was ascertained by chemical analysis using the CGHE method (Fig. 13).

The high potential of the reactive gas pressure method in the field of preparative solid state chemistry has been outlined through the examples given in this contribution. Obviously, the choice of reactive gas pressure is crucial for the selective synthesis of specific nitrogen-containing compounds. Increasing reaction pressures up to 6000 bar facilitates access to intermediates of high nitrogen content, showing that this pathway even enables the formation of single phase products that were not feasible up to now. Future work should be focused on new materials in the field of transition metal

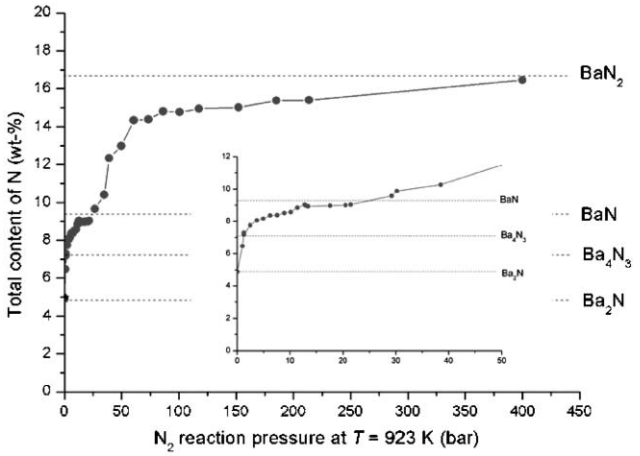


**Fig. 13** Schematic representation of phase formation in the Ba–N system controlled by the applied gas pressure. The lower pressure region is magnified in the inset. The nitrogen content was obtained from CGHE.

nitrides, in which the oxidation states of the transition metals are chosen by adjusting the redox potential of the reaction gases by variation of gas pressures.

## 6. Computational high-pressure chemistry of binary nitrides

### 6.1 Introduction

In this brief overview, we will present examples of this interaction of experiment and computation for binary nitride compounds that have originated from our group in recent years. Two exceptional examples from the literature that set landmarks in the computational chemistry of nitride compounds shall be listed. First, in 1985, McMahan and LeSar proposed the polymerization of nitrogen and, shortly after, predicted a cubic modification of nitrogen to appear above 100 GPa.[292,293] Secondly, in 2004, after numerous experimental efforts, the single-bonded cubic form of nitrogen was synthesized at temperatures above 2000 K and pressures above 110 GPa.[294] A second outstanding prediction was made for a possible superhard carbon nitride $C_3N_4$ material.[80] Although this enigmatic carbon nitride phase has not been confirmed beyond reasonable doubt, its possible existence nevertheless motivated high-pressure experiments to seek novel nitrides of higher homologues. In one of these tracks, joint experimental and theoretical work resulted in the synthesis of spinel-type $\gamma$-$Si_3N_4$ and $\gamma$-$Ge_3N_4$.[55,134]

A computational approach first starts with a model that defines the initial state and expectations about its possible development. In general, if a ground state modification of a certain composition exists, we expect a high-pressure polymorph to be denser. A higher density can be achieved in two ways: denser packing of the same structural motifs or higher (average) coordination of the constituting atoms. Coesite, a high-pressure modification of $SiO_2$, exhibits the same $SiO_4$ tetrahedra as the ground state modification of quartz, but is about 10% denser. A similar example is found for silicon nitride: the ambient pressure modifications of $\alpha$- or $\beta$-$Si_3N_4$ are

built up by $SiN_4$ tetrahedra. The hypothetical wII-$Si_3N_4$, which exhibits the same structural motif, is expected to be about 8% denser than β-$Si_3N_4$. Most often, however, higher density is achieved by higher coordination of the atoms. The standard example in silica chemistry is the transition from quartz (or coesite) to stishovite, which adopts the rutile structure, in which all Si atoms are octahedrally-coordinated. The spinel structure of $Si_3N_4$ is the corresponding example in silicon nitride chemistry. While not all Si atoms gain six-fold coordination, the ratio between the tetrahedra and octahedra is 1 : 2 and the average coordination (5.33) is 33% higher than in the ambient pressure modification of β-$Si_3N_4$.

In the following section we will outline the computational strategy used to explore the phase space for suitable candidate structures that might appear at high-pressure. Although this method is not exhaustive—nature may display even more richness than we can think of—it is nevertheless predictive.

### 6.2 Computational approach

The standard computational approach in the search for new high-pressure modifications is to compute a manifold of crystal structures and access the enthalpy as a function of pressure. In a binary system, we build a library of structures consisting of $n$ cations and $m$ anions. Note that in searching structural libraries, neither cations nor anions have to be of the same kind. Though the most simple composition is indeed $A_nX_m$, the spinel structure $A_2BX_4$, adopted for $Si_3N_4$, provides a good example where one has to think much more broadly. Next, we compute every hypothetical polymorph for the composition, and we are interested in optimizing all its structural parameters. Some care has to be taken as sometimes large distortion of the structure may appear and need to be handled appropriately. Furthermore, symmetry constraints may inhibit relaxation towards a state of lower energy. Therefore, it is often a good idea to check the validity of a new possible structure by calculating a supercell, without symmetries, or to perform a short *ab initio* molecular dynamic simulation. Once the lowest energy structure for a polymorph is computed, its energy and volume can be compared with those of other modifications. Hence, by relying on the internal energy of the ideal crystal we have, in principle, established the ground state structure for a given composition.

For every structure of interest we calculate the energy $H$ for a series of volumina around the minimum (see Fig. 14). For one, this allows us to extract the bulk modulus $B_0$ of a structure by fitting the energy–volume ($E$–$V$) data to an equation-of-state (EOS). Secondly, we use the $E$–$V$ data to calculate an enthalpy–pressure state function. The pressure $p$ is extracted from the $E$–$V$ graph by numerical differentiation: $p = -\partial E/\partial V$ and the enthalpy according to $H = E - pV$. Most often, an appropriate equation-of-state (EOS) function can be used as well to extract the pressure from the $E$–$V$ data. The EOS, however, is one parameterization function for a wide pressure range. The spline function, on the other hand, is much more robust if the system changes its behavior under compression, *e.g.*, by distortions or displacive phase transformations. Hence, using splines typically gives a more accurate

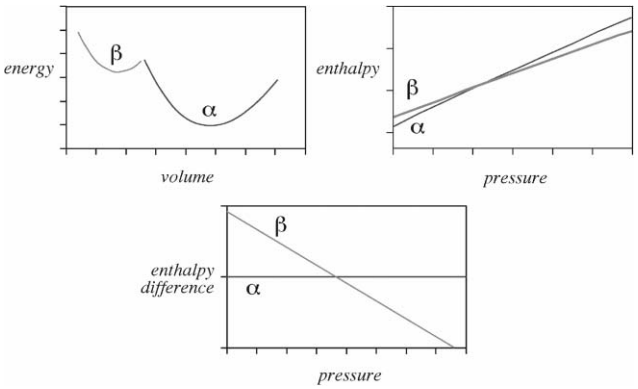


**Fig. 14** Top-left: Energy–volume ($E$–$V$) diagram for a given composition with two crystalline phases, α and β, respectively. Once an optimized structure is found, the energy is calculated for a series of volumes around the minimum. Note that the constraint of constant volume may still allow a change in the ratio of lattice constants. Top right: The $E$–$V$ data is used to calculate an enthalpy–pressure state function and to generate a $H$–$p$ diagram. The crossing of the two lines for α and β defines equal enthalpy and the point of phase transition, given unlimited time for equilibration. Bottom: In making the enthalpy–pressure data more comprehendable, it is good practice to choose a reference structure and plot the difference in enthalpy $\Delta H$ as a function of pressure $p$. Note that in our example, the enthalpy only appears to be a linear function of pressure, because of the large ratio between the bulk modulus and the pressure scale.

value for $p$. By comparing the enthalpy–pressure state functions of several polymorphs, we are now able to predict the phase with lowest enthalpy $H$ for a given pressure $p$. It is good practice to plot enthalpy differences with reference to a given phase (often the ground state). This makes the transformation pressures $p$ more easily accessible, because the crossing of the curves within the enthalpy–pressure ($\Delta H$–$p$) diagram appear at a larger scale. With the assumption that contributions of entropy to the free enthalpy are small in comparison to enthalpy differences, we calculate that the phase with lowest enthalpy $H$ will be adopted for a given pressure $p$, if thermodynamic equilibrium can be achieved. The transition pressure can also be calculated from the slope of a common tangent to the $E$–$V$ curves of the different phases. Generation of a $\Delta H$–$p$ diagram, however, has the advantage of allowing the easy estimation of the uncertainty in $p$, if an uncertainty in $\Delta H$—say due to the approximation $\Delta G \approx \Delta H$—is given.

Treating enthalpy $\Delta H$ and free enthalpy $\Delta G$ on an equal footing has its limitations though. It is important to note that the discussion of the differences in enthalpies is only relevant at absolute zero. It can be justified because the additional entropy term $T\Delta S$ is typically small in comparison to the much larger variation of $\Delta H$ within a few GPa pressure. The transformation of one phase into another, or more generally between educts and products, is then governed only by enthalpy. However, if entropy is an important property of only one of the participating phases, entropy needs to be taken into account. Such a situation arises, for example, if one of the products or educt is a gaseous species or if a phase assemblage may transform-to or develop-from a solid solution under pressure.

In general, a large variety of theoretical methods can be employed to compute energies of crystal structures in this approach. In some cases it may be enough to use simple empirical potentials to study ionic systems at high-pressure. More sophisticated electronic structure methods perform much better. Currently, state-of-the-art density functional methods have the best performance when studying the high-pressure science of semiconductors or metallic systems. However, if correlated electrons play a significant part, more advanced (and more time-consuming) methods, such as Quantum-Monte-Carlo techniques, are already available.

In particular, our computations of crystal structures are based on density functional theory, as implemented in the Vienna *Ab Initio* Simulation Package (VASP).[295–297] We employ the generalized gradient approximation (GGA) to compute energy differences. If transition metals are involved in the procedure of accessing nitrogen fugacity, we rely on Blöchl's projector augmented wave (PAW) method.[298,299] The pseudopotentials of the metal atoms include the d-electrons as valence states. The local density approximation (LDA) is used for comparison and to compute the elastic properties of the compounds. Favoring of GGA over LDA for differences in enthalpy is based on the experience that gradient corrections offer significant improvements when structures with different environments and atom coordinations are compared with each other. This has a significant impact for estimating transition pressures, as shown, for example, for $SiO_2$ and $Si_3N_4$. The cut-off energy (500 eV) for the expansion of the wave function into plane waves and the *k*-point sampling scheme is chosen to ensure that all structures are well-converged to better than 1 meV per atom.

### 6.3 Applications

**Silicon nitride, $Si_3N_4$.** Ambient pressure modifications of silicon nitride are α-$Si_3N_4$ and β-$Si_3N_4$. Both structures are related to phenacite ($Be_2SiO_4$) and can be described as an assembly of corner-sharing $SiN_4$ tetrahedra, with each three tetrahedra sharing a common corner. The α- and β-modifications have approximately the same enthalpy, both from experimental results obtained under ambient conditions and from computations up to 20 GPa. We will take β-$Si_3N_4$ as a reference structure. As noted already, it is possible to construct a second structure of $Si_3N_4$ consisting of $SiN_4$ tetrahedra. This structure is denoted willemite-II (wII) because it is derived from a high-pressure phase of zinc silicate, $Zn_2SiO_4$ (willemite). It was first proposed as a low-compressible modification of carbon nitride, $C_3N_4$.[82] Similar to α-$Si_3N_4$ and β-$Si_3N_4$, the wII structure is an assembly of corner-connected tetrahedra, with each three tetrahedra sharing a common corner. Its density, once optimized, is about 8% higher than that of β-$Si_3N_4$.

Taking a different perspective, the structures of β-$Si_3N_4$ and wII-$Si_3N_4$ are 3/4-alternating network structures with only even-membered rings. Upon investigation of a manifold of such structures, we encountered one particular network which did not retain its connectivity during optimization. Instead, it distorted into the spinel structure and hence increased the average connectivity of the cations from 4 to 5.33.

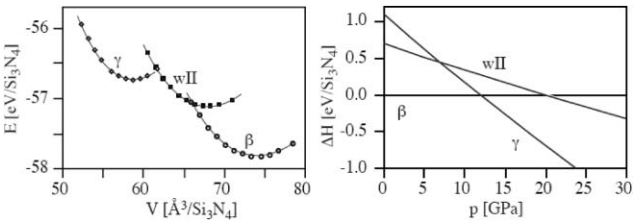


**Fig. 15** Left: Internal energy $E$ as a function of volume $V$ for the three polymorphs of $Si_3N_4$: β-, wII- and γ-$Si_3N_4$. The line in each $E$–$V$ curve is a fit to Murnaghan's equation-of-state. Right: The enthalpy–pressure diagram (taking the β-structure as the reference).

Computation of the three structures of $Si_3N_4$ yields the $E$–$V$ and $\Delta H$–$p$ diagrams shown in Fig. 15.

The $E$–$V$ graph shows that β-$Si_3N_4$ is the phase with lowest energy and highest volume. At lower volume, when the energy of β-$Si_3N_4$ increases again, the wII structure is the one with lowest energy for a molecular volume from 65 down to 61 Å$^3$. At an even smaller volume, the spinel type is the lowest energy structure. One may be tempted to interpret the graph in such a way that, upon compressing β-$Si_3N_4$, the ensemble will always adopt the structure with the lowest internal energy. However, this point of view is wrong. The $\Delta H$–$p$ diagram clearly shows that wII has no pressure range in the phase diagram over which it might become stable. The transition pressure $p_t$ of the $\beta \rightarrow \gamma$ transition is calculated to be 12 GPa. At the same time as the calculations were done, the research group were successful in synthesising spinel-type γ-$Si_3N_4$ in a DAC. The experimental transition pressure was 15 GPa at 2000 K. Later experiments using a multi-anvil press found a pressure–temperature range of 13–15 GPa and 1600–1800 °C.[138] Overall, the match between the calculated and experimental results is almost perfect, showing the applicability of the approximation $\Delta G \approx \Delta H$.

Soon after the discovery of γ-$Si_3N_4$, we set out to find further high-pressure modifications of silicon nitride. Such post-spinel phases are likely to appear; examples are high-pressure experiments on spinel ($MgAl_2O_4$) itself and magnetite ($Fe_3O_4$).[300,301] Indeed, we found no less than three possible post-spinel modifications of $Si_3N_4$ with denser packings and higher coordination numbers in comparison to γ-$Si_3N_4$: a $Ni_3Se_4$-type, a $CaTi_2O_4$-type and a (distorted) $CaFe_2O_4$-type. All three hypothetical structures become more favorable in enthalpy terms at pressures exceeding 160 GPa, with the $CaTi_2O_4$-type being the most auspicious.[302] The $CaTi_2O_4$-type of $Si_3N_4$ comprises all Si atoms six-fold coordinated to N, both in octahedra and in trigonal prisms. And indeed, in 2004, Sekine reported the experimental indication of a further high-pressure phase of spinel-type silicon nitride (and SiAlONs) that appeared above 100 GPa in dynamic shock-wave experiments.[303]

The story of silicon nitride is not over, however. We recently discovered that wII- and spinel-type structures are related by a Bain correspondence. Anions in the spinel structure are approximately on the sites of a face-centered cubic (fcc) lattice, while those of the wII structure are close to body-centered cubic (bcc).[304] The Bain strain transforms the anion sub-lattice (except for a marginal distortion of the ideal

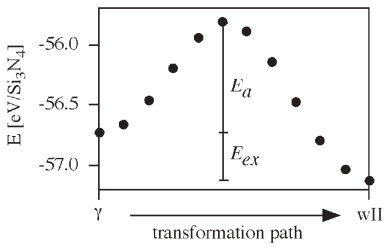


**Fig. 16** Energy profile along the transformation path from the γ- to the wII-structure of $Si_3N_4$, calculated at zero pressure. The transformation is accompanied by a change of volume and *c*/*a* ratio. For the calculations, the lattice parameters were interpolated, the cation positions kept fixed and the anion positions optimized. The activation energy $E_a$ is about 0.9 eV per $Si_3N_4$, the excess energy $E_{ex}$ equals the energy difference between the γ- and wII-structures: approximately 0.4 eV per $Si_3N_4$.

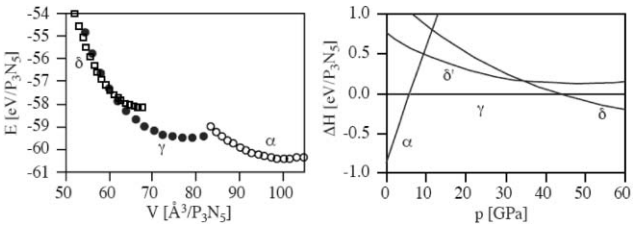


**Fig. 17** Left: The energy volume *E*–*V* diagram of $P_3N_5$, including the structures of α-, γ- and the triclinic δ-$P_3N_5$. Right: The enthalpy–pressure diagram of $P_3N_5$. Note that the enthalpy is given with reference to the γ-phase. This diagram also includes the monoclinic structure δ′.

arrangements) and two thirds of the cations, while one third of the cations are related by an additional shuffle distortion. It is possible to compute directly the activation barrier along the continuous path of this structural transformation, as shown in Fig. 16, coming out at about 0.9 eV per $Si_3N_4$. This is much lower than the energy typically associated with a bond breaking mechanism. Taken *per atom*, the energy corresponds to a temperature of about 1500 K, matching the experimental decomposition temperature of γ-$Si_3N_4$ quite closely.[305] The Bain correspondence might then be used to realize the wII-type of $Si_3N_4$ in a laboratory as well. Up to 7 GPa, wII-$Si_3N_4$ is more stable with regard to its enthalpy than γ-$Si_3N_4$. However, γ-$Si_3N_4$ can be synthesized at high-pressure and quenched to ambient conditions. If, at some pressure below 7 GPa, the transformation from wII to spinel can be initiated, the excess energy of the transformation needs to be dissipated to avoid deterioration. The spinel modification of $Si_3N_4$ may thus serve as a precursor for the synthesis of the wII modification, which is otherwise metastable throughout the enthalpy–pressure phase diagram of $Si_3N_4$ and not accessible *via* standard pressure techniques using equilibrium thermodynamics.

**Phosphorous nitride, $P_3N_5$.** By some analogy to the developments in silicon nitride, a novel high-pressure polymorph of phosphorus nitride, γ-$P_3N_5$, was synthesized.[218] While the ambient pressure modification α-$P_3N_5$ is built up by a covalent network structure of $PN_4$ tetrahedra, the high-pressure modification γ-$P_3N_5$ exhibits an increase in the coordination number of phosphorus, exhibiting tetrahedral $PN_4$ and distorted square-pyramidal $PN_5$units in a molar ratio of 1 : 2. Both polymorphs of $P_3N_5$ were studied for their behavior under high-pressures. A detailed analysis revealed a symmetry reduction of α-$P_3N_5$ from *C*2/*c* to *Cc*, already at very low pressures. *E*–*V* and Δ*H*–*p* diagrams give a transition pressure for the transition α-$P_3N_5$ → γ-$P_3N_5$ of 6.2 GPa. The experimental conditions of the synthesis were reported to be 11 GPa and 1500 °C.[218] This appears to be only a fair agreement between experimental and computational results. It has to be realized, however, that the experimental value is an upper boundary of the pressure needed to invoke the transformation, while more experiments to locate the phase boundary have not been carried out as well as for silicon nitride.

Interestingly, yet another high-pressure modification of $P_3N_5$ is within experimental reach. Utilizing the structural variety of $Al_2SiO_5$ and $MSi_2O_5$ (M = Mg, Ca), which display a rich high-pressure chemistry themselves, we studied structures that comprise a higher average coordination than γ-$P_3N_5$.[306] Very similar results were obtained by another group as well, who proposed a sillimanite-type phase as a further high-pressure modification of $P_3N_5$.[307] The most promising candidate for a δ-$P_3N_5$ we found is isotypic to kyanite, an $Al_2SiO_5$ modification. It comprises $PN_6$ octahedra-sharing edges, while isolated $PN_4$ tetrahedra share vertices with octahedra. This situation is very similar to spinels, hence resembling the high-pressure chemistry of silicon nitride. The triclinic Kyanite-type of $P_3N_5$ will succeed γ-$P_3N_5$ at pressures above 43 GPa (see Fig. 17). However, it will not be stable at lower pressures, but instead will most likely distort into a monoclinic structure, denoted δ′-$P_3N_5$, with significantly lower enthalpy below 34 GPa. δ′-$P_3N_5$ comprises $PN_6$ octahedra, $PN_5$ trigonal-bipyramids, as well as $PN_4$ tetrahedra, and is not structurally related to any of the $Al_2SiO_5$ or $CaSi_2O_5$ polymorphs. The monoclinic and triclinic structure are related by a shear distortion, which makes this transition likely to happen during the process of quenching. Within the given limitations—as we cannot access, at elevated temperatures, the contributions of entropy to the free energy of the decomposition—we conclude that the appearance of a further high-pressure phase of $P_3N_5$ is very likely and that the P–N phase diagram still offers some new aspects.

**Hafnium nitride, $Hf_3N_4$.** It did not take long before new binary metal nitrides were realized. The first example, cubic hafnium(IV) nitride, $Hf_3N_4$, with a thorium phosphide $Th_3P_4$-type structure, was synthesized at 18 GPa and 2800 K in a DAC from elemental hafnium and nitrogen.[77] This endeavour was especially important because the high-pressure route yielded a phase of this composition for the first time. Experiments on the synthesis of cubic zirconium(IV) nitride were analogous and yielded the isostructural compound at 15.6–18 GPa and 2500–3000 K. An ambient pressure modification of orthorhombic structure was known previously for $Zr_3N_4$.[176] The $Th_3P_4$-type structure comprises the cation in eight-fold coordination, and the two new compounds were the first binary nitrides exhibiting an $MN_8$ motif.

 

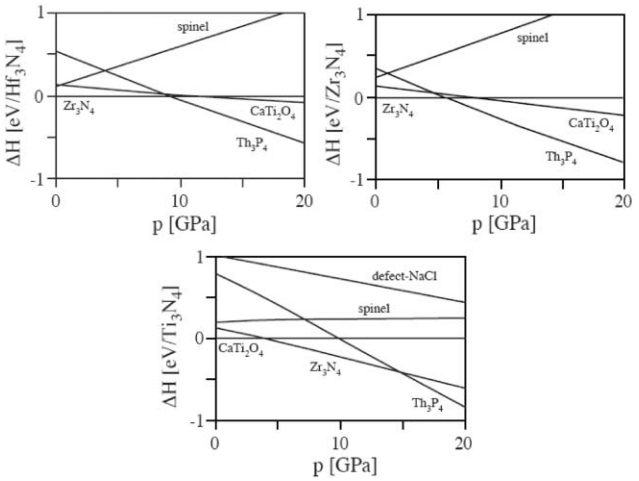


**Fig. 18** Enthalpy–pressure ($\Delta H$–$p$) phase diagrams of $Hf_3N_4$ (top left), $Zr_3N_4$ (top right) and $Ti_3N_4$ (bottom). Note that an orthorhombic $Zr_3N_4$-type structure constitutes the ground state of $Hf_3N_4$ and $Zr_3N_4$ while a $CaTi_2O_4$-type is the ground state of $Ti_3N_4$.

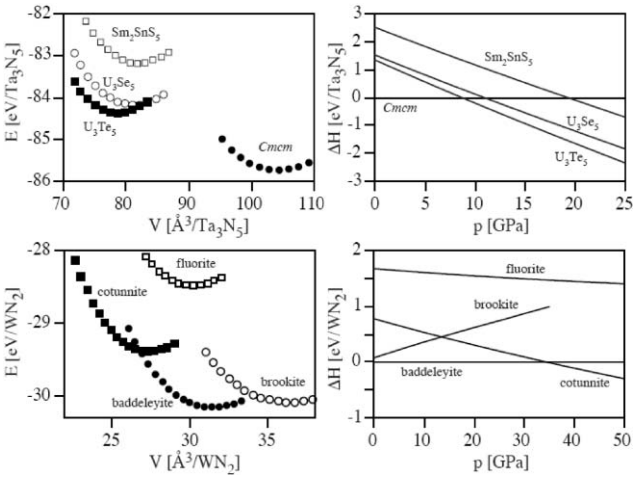


**Fig. 19** Energy–volume $E$–$V$ (left) and enthalpy–pressure $\Delta H$–$p$ (right) diagrams for various crystal structures of $Ta_3N_5$ (top) and $WN_2$ (bottom).

For the calculation, we could exploit the library of structures we had accumulated for silicon nitride and compute a manifold of possible modifications. Interestingly, for both $Hf_3N_4$ and $Zr_3N_4$, the orthorhombic structure is the one with the lowest energy.[308] Hence, an orthorhombic $Hf_3N_4$ will exist, in analogy to $Zr_3N_4$, but has not yet been synthesized. Between orthorhombic- and $Th_3P_4$-types of $Hf_3N_4$ we found no less than five other candidates with energies lower than that of the $Th_3P_4$-type of $Hf_3N_4$: spinel, $CaTi_2O_4$, $Yb_3N_4$, $Sr_2Pb_2O_4$ and $CaFe_2O_4$. For $Zr_3N_4$, only three of these have energies between those of the orthorhombic ground state and the $Th_3P_4$-type: $CaTi_2O_4$, $Yb_3N_4$ and spinel. However, none of these structures has a pressure range where it will be lower in enthalpy than the orthorhombic ground state, although $Yb_3N_4$ and $CaFe_2O_4$ have a higher average coordination than the ground state. They are all outperformed by the $Th_3P_4$-type. We calculate that the orthorhombic- $\rightarrow$ $Th_3P_4$-type transition will occur at 9 and 6 GPa for $Hf_3N_4$ and $Zr_3N_4$, respectively (see Fig. 18). For $Ti_3N_4$, the situation is somewhat different. Here, the $CaTi_2O_4$-type comes out slightly lower in energy than the orthorhombic-type $Zr_3N_4$, but may transform into this at about 4 GPa.[309] The orthorhombic- $\rightarrow$ $Th_3P_4$-type transition of $Ti_3N_4$ will take place at 15 GPa.

**Tantalum nitride, $Ta_3N_5$, and tungsten dinitride, $WN_2$.** In a similar way, we carried out our research on new high-pressure modifications of tantalum(V)- and tungsten(VI) nitride.[310] The orthorhombic structure of $Ta_3N_5$ is computed as the lowest energy among a great variety of (hypothetical) polymorphs. Once again, by scanning a manifold of possible structures, we found several candidate structures which might be adopted at higher pressure. The most promising candidate we found is isostructural to $U_3Te_5$. While the orthorhombic structure comprises each tantalum atoms in six-fold coordination to nitrogen, the $U_3Te_5$-type polymorph of $Ta_3N_5$ exhibits tantalum in eight-fold coordination. This compares well with the eight-fold coordination of Hf atoms in cubic $Hf_3N_4$.[77] Energy–volume and enthalpy–pressure phase diagrams of $Ta_3N_5$, displayed in Fig. 19, show that the orthorhombic ground state is the most stable polymorph of $Ta_3N_5$ up to 9 GPa. Above this pressure, the $U_3Te_5$-type is favored. Hence, neglecting the differences in entropy, we expect a new modification of $Ta_3N_5$ to appear above 9 GPa.

The case of tungsten(VI) nitride is more difficult because no crystal structure of $WN_2$ is known so far. Though nitrogen-rich $WN_x$ thin films, with a composition close to $WN_2$, can be produced by low-temperature deposition methods, a crystalline modification still awaits its realization. If it exists, structures of ground state and high-pressure modifications will be very similar to those of $ZrO_2$. A monoclinic baddeleyite-type structure of $WN_2$ comes out as the lowest in energy (see Fig. 19).[310] It comprises tungsten in seven-fold coordination to nitrogen, forming $WN_7$ mono-capped trigonal prisms. We computed a cotunnite-type $WN_2$ to be the most likely candidate for a high-pressure modification. In this structure, tungsten will be in nine-fold coordination to nitrogen, forming tri-capped trigonal prisms. A fluorite-type structure of $WN_2$ will not play a role in the phase diagram, although very early speculations designated this phase as a likely type of $WN_2$.[311] The computed energy–volume and enthalpy–pressure phase diagrams for $WN_2$ show that the baddeleyite-type is the most stable polymorph of $WN_2$ up to a pressure of 34 GPa, above which it transforms into the cotunnite-type.

### 6.4 Nitridation at high-pressure and temperature—fugacity of nitrogen

Calculations of binary nitrides of constant composition can be very useful if a low-pressure modification is known that may be used as a precursor for a high-pressure experiment. Hence, for $Zr_3N_4$ or $Ta_3N_5$, experiments can take advantage of it. However, synthesising a new nitride compound from the elements at high temperatures and pressures necessitates additional computation to estimate the pressure needed for a successful experiment. For example, the calculated enthalpy data for $Hf_3N_4$ or $Zr_3N_4$ do not explain the experimental conditions necessary to synthesize the $Th_3P_4$-type, 16 GPa and

2800 K. The chemical route to $Hf_3N_4$ in a DAC started with metal platelets or cold-pressed powder pellets of the mono-nitride HfN as precursors. These were embedded in nitrogen, which was not only a reactant but also the pressure medium, and then squeezed to the desired pressure. The cell was heated with laser radiation to activate the transformation. Under such conditions, we will eventually face the problem that a solid nitride compound will decompose with development of nitrogen. Therefore, in comparison to a system of constant composition, in which the enthalpy difference $\Delta H$ between structures provides a good measure to derive a phase diagram at elevated pressure, an open system, in which one of the reactants is a gaseous species, is inherently more complicated.

To make our point clear: if heated, $Ta_3N_5$ starts to decompose into TaN and nitrogen gas through a series of intermediate compositions at about 1000 °C at ambient pressure.[312] The entropy of the gas at high temperatures shifts the equilibrium towards the mono-nitride. However, a high-temperature is most often needed to activate the transformation towards a denser polymorph. Hence, we may need a significantly higher pressure for synthesising the novel modification to prevent its immediate decomposition. Essentially, what we need is an assessment of the activity of nitrogen at high temperatures and pressures. The approach we recently proposed is to combine *ab initio* density functional calculations with semi-empirical thermochemical calculations. Central in this approach is the equilibrium between educt and nitridation product. For example, for hafnium nitride, we consider the reaction between mono-nitride and the fully oxidized metal nitride (eqn. 3):

$$3\ \mathrm{HfN} + 0.5\ \mathrm{N_2} \leftrightarrow \mathrm{Hf_3N_4} \quad (3)$$

$$\Delta G(\mathrm{p,T}) = \Delta H^{\mathrm{sol}}(\mathrm{p}) + \Delta G^{\mathrm{gas}}(\mathrm{p,T}) \quad (4)$$

In this first order approximation of $\Delta G$ (eqn. 4), we reflect the fact that, at elevated temperatures, the formation of gaseous nitrogen contributes the most to the free enthalpy of formation, $\Delta G$. Differences in entropy between the solid state compounds contribute significantly less. That leaves us with the problem of finding appropriate data for $\Delta G(\mathrm{p,T})$. At ambient pressure, the free enthalpy of nitrogen is tabulated in thermochemical tables for temperatures up to 4000 K.[313] If nitrogen is treated as an ideal gas, the residual pressure dependence of $\Delta G$ can be computed according to the standard formula (eqn. 5):

$$\Delta G(\mathrm{p,T}) = \Delta G(p = 0,\mathrm{T}) + RT \ln p \quad (5)$$

This was indeed the approach we used to derive the temperature–pressure phase diagram for $Hf_3N_4$ and $Zr_3N_4$.[308]

Significant improvements for pressures exceeding 20 GPa are necessary because the deviation of nitrogen from ideal gas behavior becomes more and more drastic. Note that at such temperatures and pressures, nitrogen is in an over-critical state anyway (the critical point of $N_2$ being at about 126 K and 3.44 MPa) so there is no difference between its gaseous and liquid states. To recover the simple formula of eqn. 5, the true pressure is replaced by an effective pressure called fugacity, $f$. Fugacity and pressure are related by the fugacity coefficient, $\gamma$, through the relationship $f = \gamma p$; if $\gamma = 1$, the gas is in an ideal state. Unfortunately, the pressure dependencies of $\gamma$ and $\Delta G$ are known experimentally only up to 2 GPa. Jacobsen *et al.* collected experimental data about nitrogen properties from the freezing line up to 2000 K and for pressures up to 1 GPa. Unland *et al.* developed a virial expansion for ln $\gamma$ based on this experimental data, but it is valid only up to 2 GPa.[314,315] Most remarkably, at 300 K and 2 GPa, the fugacity coefficient is about $10^6$ (ln $\gamma$ = 20). Hence, the effective pressure for nitrogen is 6 orders of magnitude larger than the pressure applied. At higher temperatures, the behavior becomes more and more "ideal", but even at 2000 K and 2 GPa, the effective pressure is 20 times larger than the actual pressure. With our aim of computing temperature–pressure phase diagrams at even higher pressures, we extrapolated the virial expansion in a reasonable and justifiable way. We proposed two extrapolations, which may serve as low- and high-profile estimates of $f$, and thus provide boundaries for predictions. Details of both functional forms are given in ref. 310; the graph of ln $\gamma$ *vs.* pressure is shown for two temperatures in Fig. 20.

Derivation of the phase boundary between the mono-nitride and the fully oxidized metal nitride then becomes simple. According to eqn. 4, we first compute the enthalpies of the crystal structures and then add the contribution of the free enthalpy of nitrogen to obtain the free enthalpy of reaction, $\Delta G$. Note that in our own interests, only the regime above 1000 K and 2 GPa is of importance. With the location of the phase boundary, we can plot the pressure–temperature ($p$–$T$) phase diagram. Fig. 21 shows these for Ta–N and W–N, respectively. Accordingly, we predict the formation of $Ta_3N_5$-II in a DAC experiment between 17 and 25 GPa at 2800 K. At the same temperature, $WN_2$-II can be synthesized between 31 and 55 GPa.

We applied the same approach to the carbon–nitrogen phase diagram, in detail to the balance between the proposed cubic willemite-type phase c-$C_3N_4$ and diamond + nitrogen. Fig. 22 shows the estimated phase boundary. From it we can learn that if temperatures of 3000–3500 K are applied (typical for the synthesis of diamond from graphite), not less than 100 GPa is needed to reach an equilibrium between the products and the educt. In this pressure range, we would have to consider the formation of cubic nitrogen, which we did not take into account in our estimation. Once a $C_3N_4$ material has been

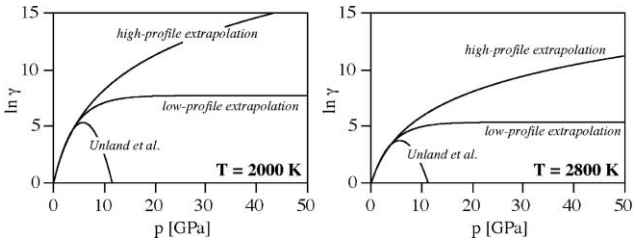


**Fig. 20** Logarithm of the fugacity coefficient, ln $\gamma$, plotted as a function of pressure for 2000 (left) and 2800 (right) K. The virial expansion of Unland *et al.* shows an artificial decrease at higher pressures, since it is valid up to 2 GPa only. High- and low-profile extrapolations have been developed to justifiably estimate ln $\gamma$ at very high pressures.

 

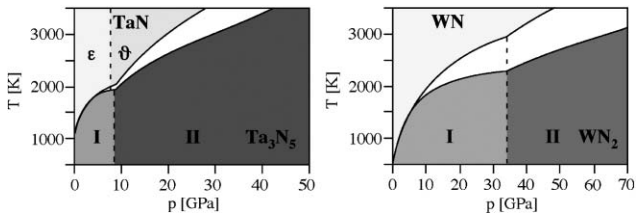


**Fig. 21** Left: The computed pressure–temperature phase diagram of Ta–N showing the boundary between the compositions TaN and $Ta_3N_5$, using high profile (upper line) and low-profile (lower line) expansion for the fugacity of nitrogen. Right: A similar $p$–$T$ phase diagram of W–N, including WN and $WN_2$. The dashed lines separate phases of the same composition.

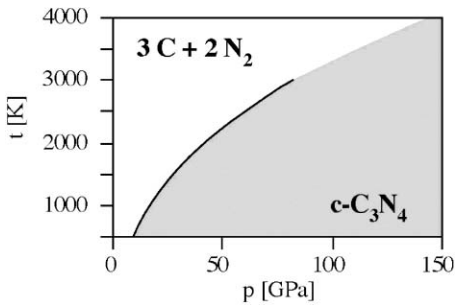


**Fig. 22** Computed phase boundary between the cubic phase of $C_3N_4$ and diamond + nitrogen. An average of high and low profile expansion for the fugacity of nitrogen is used. The black line, which separates the regions of thermodynamic stability, is given up to 70 GPa only due to the functional form.

synthesized by some method or the other, it turns out to be thermodynamically stable (against decomposition into diamond and nitrogen) at 2000 K and 40 GPa. This motivates the synthesis of $C_3N_4$ from suitable carbon nitride precursors under such conditions. At ambient pressure, a significant kinetic barrier can keep the compound metastable.

### 6.5 Summary and outlook

In this review we referred to a computational procedure for studying the perspectives of novel nitride compounds that may become accessible at high pressures. The scheme we outlined can be applied to any nitride compound. If we estimate the uncertainty of the computational approach by comparing the calculated transition pressures to experimental values, we find some 2–5 GPa for calculations at constant composition. Uncertainty with the nitridation reaction is larger, and we estimate a generous margin of 5 GPa and 300 K. Since our extrapolation of thermochemical data is based on a low pressure regime, the uncertainty gets larger at greater experimental pressures. Nevertheless, the combination of first principle and thermodynamical calculations, according to the proposed scheme, allows an assessment of free enthalpies and the computation of a full temperature–pressure phase diagram. We now can work out the $p$–$T$ range for a successful experiment and provide this data to the experimental community to stimulate their efforts. Moreover, such calculations provide enough accuracy to validate experimental hypotheses.

Improvements leading to better calculations can be achieved with an experimental assessment of nitrogen properties beyond 2 GPa. In principle, data from nitridation reactions, such as the recent endeavour in platinum nitride compounds PtN and $PtN_2$, and the nitridation of Co to $Co_2N$, also yield conclusions on nitrogen fugacity.[182,183,316] Overall, joint experimental and computational work will result in the discovery of further new nitride compounds, and there remains much to do in high-pressure research.

## 7. Conclusion and outlook

A series of new binary and ternary compounds based on nitrides, oxonitrides, nitride-imides and nitride-diazenides have been successfully synthesized in recent years by applying different high pressure/high temperature techniques including large volume press (*e.g.*, multi-anvil), laser heated diamond anvil cells, shock wave methods and pressurized reactive gas synthesis. It has been shown that under high pressure novel materials with unusual structural features can be formed. In general, as has already found for silicate minerals and other oxides, the coordination number of the constituent elements is increased compared to the analogous ambient pressure phases. The increase in the coordination number has significant consequences in terms of the hybridization or ionicity of the bonding between individual atoms that determine technologically important properties such as the electronic structure and mechanical behavior of the solid phase, including, in turn, electronic properties such as the electronic band gap and elastic properties like the bulk and shear modulus ($B$ and $G$, respectively) and the hardness. As a general trend among the nitrides it is found that the band gap is reduced while the elastic moduli are increased in the high pressure phases compared to the values found for the ambient pressure counterparts. These features lead to new materials prepared using high-pressure techniques with technologically useful properties. At present, only a few studies related to the high pressure/high temperature synthesis of main group and transition group element nitride, oxonitride and related compounds have been reported. Furthermore, apart from the binary compositions, the syntheses of ternary and more complex systems as well as their $P$–$T$ phase diagrams have still to be explored in any detail. Detailed studies of the reaction kinetics that dominate under high pressure conditions must also be performed in future in order to understand the formation and phase transformations of the unique high pressure phases, both during synthesis and to establish recovery strategies for the new materials.

## Acknowledgements

Ralf Riedel and Andreas Zerr acknowledge the DFG, Bonn, Germany, for continuous support in the field of high-pressure materials chemistry over the past 10 years. Ralf Riedel thanks the DFG for founding a new priority research program entitled "Synthesis, In Situ Characterisation and Quantum Mechanical Modeling of Earth Materials, Oxides, Carbides and Nitrides at Extremely High Pressures and Temperatures" (DFG-SPP 1236). High-pressure research in the group of Paul

F. McMillan in London is supported by the EPSRC (Portfolio award EP/D504782/1). McMillan is a Wolfson-Royal Society Research Merit Award Fellow. Andreas Zerr appreciates the honour of the Adolf-Messer-Pries, received in 2004 for his high-pressure research. Peter Kroll thanks the DFG for financial support (contracts Kr1805/5-1 and Kr1805/9-1). The computational work was made possible by very generous grants from the Forschungszentrum Jülich and the Center for Computation and Communication, Aachen. The authors acknowledge the helpful comments of John Tse. The editing of the multi-anvil apparatus details was carried out by Dmytro Dzivenko.

## References


1 P. W. Bridgman, *The Physics of High Pressure*, G. Bell & Sons, London, 1931.
2 P. F. McMillan, *Nat. Mater.*, 2005, **4**, 715.
3 R. M. Hazen, *The Diamond Makers*, Cambridge University Press, Cambridge, 1999.
4 L.-G. Liu and W. A. Bassett, *Elements, Oxides, Silicates: High Pressure Phases with Implications for the Earth's Interior*, Oxford University Press, London, 1986.
5 P. F. McMillan, *Nat. Mater.*, 2002, **1**, 19.
6 R. Boehler, *Rev. Geophys.*, 2000, **38**, 221.
7 P. F. McMillan, *Chem. Commun.*, 2003, 919.
8 L. Davison, Y. Hori and T. Sekine, *Shock Compression of Solids*, New York, Springer-Verlag, 2002.
9 V. E. Fortov, L. V. Al'tshuler, R. F. Trunin and A. I. Funtikov, *Shock Waves and Extreme States of Matter*, New York, Springer-Verlag, 2004.
10 N. Subrahama, *J. Sci. Ind. Res.*, 1972, **31**, 241.
11 T. Sekine and T. Kobayashi, *New Diamond Front. Carbon Technol.*, 2003, **13**, 153.
12 P. F. McMillan, *High Pressure Res.*, 2003, **23**, 7.
13 V. L. Solozhenko, *High Pressure Res.*, 2004, **24**, 499.
14 P. V. L. Solozhenko, *High Pressure Res.*, 2002, **22**, 519.
15 S. Nakamura, *MRS Bull.*, 1997, **22**, 29.
16 F. A. Ponce and D. P. Bour, *Nature*, 1997, **386**, 351.
17 N. E. Brese and M. O'Keeffe, *Struct. Bonding*, 1992, **79**, 307.
18 F. J. Disalvo, *Mater. Sci. Forum*, 2000, **383**(3–9), 325.
19 W. Schnick, *Angew. Chem., Int. Ed. Engl.*, 1993, **32**, 806.
20 A. Zerr and R. Riedel, in *Handbook of Ceramic Hard Materials*, ed. R. Riedel, Wiley-VCH, Weinheim, 2000, Part 1, pp. XLV—LXXIII.
21 R. Riedel, *Adv. Mater.*, 19994, **6**, 549.
22 W. Bronger and G. Auffermann, *Chem. Mater.*, 1998, **10**, 2723.
23 G. Auffermann, R. Kniep and W. Bronger, *Z. Anorg. Allg. Chem.*, 2006, **632**, 565.
24 F. R. Boyd and J. L. England, *J. Geophys. Res., [Atmos.]*, 1960, **65**, 741.
25 E. Ohtani, N. Kagawa, O. Shimomura, M. Togaya, K. Suito, A. Ondera, H. Sawamoto, M. Yoneda, S. Tanak, W. Utsumi, E. Ito, A. Matsumoto and T. Kikegawa, *Rev. Sci. Instrum.*, 1989, **60**, 922.
26 T. Kondo, H. Sawamoto, A. Yoneda, M. Kato, A. Matsumoto and T. Yagi, *High Temp.-High Pressures*, 1993, **25**, 105.
27 T. Irifune, H. Naka, T. Sanehira, T. Inoue and K. Funakoshi, *Phys. Chem. Miner.*, 2002, **29**, 645.
28 R. van Eldik and F.-G. Klärner, *High Pressure Chemistry: Synthetic, Mechanistic, and Supercritical Applications*, Wiley-VCH, Weinheim, 2002.
29 J. Chen, Y. Wang, T. S. Duffy, G. Shen and L. P. Dobrzhinetskaya, *Advances in High-Pressure Technology For Geophysical Applications*, Elsevier, Amsterdam, 2005.
30 M. I. Eremets, *High Pressure Experimental Methods*, Oxford University Press, London, 1995.
31 W. Holzapfel and N. S. Isaacs, *High Pressure Techniques In Chemistry and Physics: A Practical Approach*, Oxford University Press, London, 1997.
32 *Reviews in Mineralogy: Ultrahigh-Pressure Mineralogy: Physics and Chemistry of the Earth's Deep Interior*, ed. R. J. Hemley, University of Chicago Press, Chicago, 1998, vol. **37**.
33 D. Walker, M. A. Carpenter and C. M. Hitch, *Am. Mineral.*, 1990, **75**, 1020.
34 M. J. Walter, Y. Thibault, K. Wei and R. W. Luth, *Can. J. Phys.*, 1995, **73**, 273.
35 D. C. Rubie, *Phase Transitions*, 1999, **68**, 431.
36 H. Huppertz, *Z. Kristallogr.*, 2004, **219**, 330.
37 D. J. Frost, B. T. Poe, R. G. Trønnes, C. Liebske, A. Duba and D. C. Rubie, *Phys. Earth Planet. Inter.*, 2004, **143–144**, 507.
38 A. Neuhaus, *Chimia*, 1964, **18**, 93.
39 A. Jayaraman, W. Lowe and L. D. Longinotti, *Phys. Rev. Lett.*, 1976, **36**, 366.
40 C. E. Weir, E. R. Lippincott, A. Van Valkenburg and E. N. Bunting, *J. Res. Natl. Bur. Stand., Sect. A*, 1959, **63**, 55.
41 E. R. Lippincott, F. E. Welsh and C. E. Weir, *Anal. Chem.*, 1961, **33**, 137.
42 J. C. Jamieson, A. W. Lawson and N. D. Nachtrieb, *Rev. Sci. Instrum.*, 1959, **30**, 1016.
43 A. L. Ruoff, H. Xia and Q. Xia, *Rev. Sci. Instrum.*, 1992, **63**, 4342.
44 R. M. Hazen and L. W. Finger, *Comparative Crystal Chemistry*, John Wiley & Sons Ltd., New York, 1982.
45 A. Jayaraman, *Rev. Mod. Phys.*, 1983, **55**, 65.
46 A. Jayaraman, *Rev. Sci. Instrum.*, 1986, **57**, 1013.
47 *Gmelin's Handbuch der Anorganischen Chemie: Kohlenstoff*, Verlag Chemie, Weinheim, 1967.
48 W. L. Wolfe and G. J. Zissis, *The Infrared Handbook*, Environmental Research Institute of Michigan, Washington, DC, 1985.
49 R. A. Forman, G. J. Piermarini, J. D. Barnett and S. Block, *Science*, 1972, **176**, 284.
50 H.-K. Mao, P. M. Bell, J. W. Shaner and D. J. Steinberg, *J. Appl. Phys.*, 1978, **49**, 3276.
51 H. K. Mao, J. Xu and P. M. Bell, *J. Geophys. Res.*, 1986, **91**, 4673.
52 L. Ming and W. A. Bassett, *Rev. Sci. Instrum.*, 1974, **45**, 1115.
53 C.-S. Yoo, J. Akella and M. Nicol, in *Adv. Mater.-96, Proc. Int. Symp. 3rd, (ISAM '96)*, National Institute for Research in Inorganic Materials, Tsukuba, Japan, 1996, pp. 175–179.
54 R. Boehler and A. Chopelas, *Geophys. Res. Lett.*, 1991, **18**, 1147.
55 A. Zerr, G. Miehe, G. Serghiou, M. Schwarz, E. Kroke, R. Riedel, H. Fueß, P. Kroll and R. Boehler, *Nature*, 1999, **400**, 340.
56 R. Boehler, *Rev. Geophys.*, 2000, **38**, 221.
57 A. Zerr, G. Serghiou and R. Boehler, in *Handbook of Ceramic Hard Materials*, ed. R. Riedel, Wiley-VCH, Weinheim, 2000, Part 1, pp. 41–65.
58 A. Zerr, G. Serghiou, R. Boehler and M. Ross, *High Pressure Res.*, 2006, **26**, 23.
59 L. R. Benedetti and P. Loubeyre, *High Pressure Res.*, 2004, **24**, 423.
60 M. Planck, *Ann. Phys.*, 1900, **1**, 719.
61 D. L. Heinz, J. S. Sweeney and P. Miller, *Rev. Sci. Instrum.*, 1991, **62**, 1568.
62 A. Zerr and R. Boehler, *Science*, 1993, **262**, 553.
63 R. Boehler, N. von Bargen and A. Chopelas, *J. Geophys. Res.*, 1990, **95**, 21731.
64 D. Heinz, E. Knittle, J. S. Sweeney, Q. Williams and R. Jeanloz, *Science*, 1994, **264**, 279.
65 R. Boehler and A. Zerr, *Science*, 1994, **264**, 280.
66 G. Fiquet, D. Andrault, J. P. Itie, P. Gillet and P. Richet, *Phys. Earth Planet. Inter.*, 1996, **95**, 1.
67 G. Fiquet and D. Andrault, *J. Synchrotron Radiat.*, 1999, **6**, 81.
68 D. Andrault and G. Fiquet, *Rev. Sci. Instrum.*, 2001, **72**, 1283.
69 G. Shen, M. L. Rivers, Y. Wang and S. R. Sutton, *Rev. Sci. Instrum.*, 2001, **72**, 1273.
70 M. J. Walter and K. T. Koga, *Phys. Earth Planet. Inter.*, 2004, **143–144**, 541.
71 E. Schultz, M. Mezouar, W. Crichton, S. Bauchau, G. Blattmann, D. Andrault, G. Fiquet, R. Boehler, N. Rambert, B. Sitaud and P. Loubeyre, *High Pressure Res.*, 2005, **25**, 71.
72 R. Boehler, *Mater. Today*, 2005, 34.
73 A. S. Zinn, D. Schiferl and M. F. Nicol, *J. Chem. Phys.*, 1987, **87**, 1267.
74 M. Eremets, K. Takemura, H. Yusa, D. Goldberg, Y. Bando and K. Kurashima, *Adv. Mater.-96, Proc. Int. Symp. 3rd, (ISAM '96)*,


 

National Institute for Research in Inorganic Materials, Tsukuba, Japan, 1996, p. 169.
75 M. Bockowski, *Physica B (Amsterdam)*, 1999, **265**, 1.
76 S. Bodea and R. Jeanloz, *J. Appl. Phys.*, 1989, **65**, 4688.
77 A. Zerr, G. Miehe and R. Riedel, *Nat. Mater.*, 2003, **2**, 185.
78 T. Sekine, *Eur. J. Solid State Inorg. Chem.*, 1997, **34**, 823.
79 M. L. Cohen, *Phys. Rev. B: Condens. Matter*, 1985, **32**, 7988.
80 A. Y. Liu and M. L. Cohen, *Science*, 1989, **245**, 841.
81 A. Y. Liu and M. L. Cohen, *Phys. Rev. B: Condens. Matter*, 1990, **41**, 10727.
82 D. M. Teter and R. J. Hemley, *Science*, 1996, **271**, 53.
83 A. Liu and R. M. Wentzcovitch, *Phys. Rev. B: Condens. Matter*, 1994, **50**, 10362.
84 Y. Guo and W. A. Goddard, *Chem. Phys. Lett.*, 1995, **237**, 72.
85 P. H. Fang, *J. Mater. Sci. Lett.*, 1995, **14**, 536.
86 K. Bewilogua, *Le Vide: Sci. Tech. Appl.*, 1996, **52**, 213.
87 S. Matsumoto, E. Q. Xie and F. Izumi, *Diamond Relat. Mater.*, 1999, **8**, 1175.
88 S. Muhl and J. M. Mendez, *Diamond Relat. Mater.*, 1999, **8**, 1809.
89 T. Malkow, *Mater. Sci. Eng.*, 2001, **A292**, 112.
90 E. Kroke and M. Schwarz, *Coord. Chem. Rev.*, 2004, **248**(5–6), 493.
91 A. Karimi and R. Kurt, *Surf. Eng.*, 2001, **17**, 99.
92 D. Zhong, S. Liu, G. Y. Zhang and E. G. Wang, *J. Appl. Phys.*, 2001, **89**, 5939.
93 W. Yu, G. B. Ren, S. F. Wang, L. Han, X. W. Li, L. S. Zhang and G. S. Fu, *Thin Solid Films*, 2002, **402**, 55.
94 M. Lejeune, O. Durand-Drouhin, K. Zellama and M. Benlahsen, *Solid State Commun.*, 2001, **120**, 337.
95 T. Szorenyi, J. P. Stoquert, J. Perierre, F. Antoni and E. Fogarassy, *Diamond Relat. Mater.*, 2001, **10**, 2107.
96 I. Alves, G. Demazeau, B. Tanguy and F. Weil, *Solid State Commun.*, 1999, **109**, 697.
97 M. R. Wixom, *J. Am. Ceram. Soc.*, 1990, **73**(7), 1973.
98 J. C. Fitzmaurice, A. L. Hector and I. P. Parkin, *J. Chem. Soc., J. Chem. Soc., Dalton Trans.*, 1993, 2435.
99 J. B. Wiley and R. B. Kaner, *Science*, 1992, **255**, 1093.
100 Y. Xie, Y. Qian, W. Wang, S. Zhang and Y. Zhang, *Science*, 1996, **272**, 1926.
101 C. H. Wallace, T. K. Reynold and R. B. Kaner, *Chem. Mater.*, 1999, **11**, 2299.
102 D. R. Miller, J. Wang and E. G. Gillan, *J. Mater. Chem.*, 2002, **12**, 2463.
103 V. N. Khabashesku, J. L. Zimmerman and J. L. Margrave, *Chem. Mater.*, 2000, **12**, 3264.
104 T. Komatsu and T. Nakamura, *J. Mater. Chem.*, 2001, **11**, 474; T. Komatsu, *J. Mater. Chem.*, 2001, **11**, 802.
105 J. Martin-Gil, F. J. Martin-Gil, M. Sarikaya, M. Qian, M. Jose-Yacaman and A. Rubio, *J. Appl. Phys.*, 1997, **81**, 2555.
106 J. L. Zimmerman, R. Williams, V. N. Khabashesku and J. L. Margrave, *Russ. Chem. Bull.*, 2001, **50**, 2020.
107 E. Kroke, M. Schwarz, E. Horvath-Bordon, P. Kroll, B. Noll and A. Norman, *New J. Chem.*, 2002, **26**, 508.
108 B. Jürgens, E. Irran, J. Senker, P. Kroll, H. Müller and W. Schnick, *J. Am. Chem. Soc.*, 2003, **125**, 10288.
109 E. Horvath-Bordon, E. Kroke, I. Svoboda, H. Fueß, R. Riedel, N. Sharma and A. K. Cheetham, *Dalton Trans.*, 2004, 3900.
110 R. Riedel, E. Horvath-Bordon, S. Nahar-Borchert and E. Kroke, *Key Engin. Mater.*, 2003, **247**(Advanced Ceramics and Composites), 121.
111 E. Horvath-Bordon, E. Kroke, I. Svoboda, H. Fuess and R. Riedel, *New J. Chem.*, 2005, **29**, 693.
112 J. L. Zimmerman, R. Williams, V. N. Khabashesku and J. L. Margrave, *Nano Lett.*, 2001, **1**, 731.
113 B. Molina and L. E. Sansores, *Mod. Phys. Lett. B*, 1999, **13**, 193.
114 H. Montigaud, B. Tanguy, G. Demazeau, I. Alves and S. Courjault, *J. Mater. Sci.*, 2000, **35**, 2547.
115 Z. Zhang, K. Leinenweber, M. Bauer, L. A. J. Garvie, P. F. McMillan and G. H. Wolf, *J. Am. Chem. Soc.*, 2001, **123**, 7788.
116 S. Courjault, B. Tanguly and G. Demazeau, *C. R. Acad. Sci., Ser. IIc: Chim.*, 1999, **9-10**, 487.
117 H. A. Ma, X. P. Jia, P. W. Zhu, W. L. Guo, X. B. Guo, Y. D. Wang, S. Q. Li, G. T. Zou, G. Zhang and P. Bex, *J. Phys.: Condens. Matter*, 2002, **14**, 11269.
118 V. P. Dymont, E. M. Nekrashevich and M. Starchenko, *JETP Lett. Engl. Transl.*, 1998, **68**, 498.
119 V. P. Dymont, E. M. Nekrashevich and M. Starchenko, *Solid State Commun.*, 1999, **111**, 443.
120 V. P. Dymont and I. Smurov, *Mater. Sci. Eng., B*, 2001, **82**, 39.
121 A. Andreyew, M. Akaishi and D. Golberg, *Diamond Relat. Mater.*, 2002, **11-12**, 1885.
122 A. Andreyew, M. Akaishi and D. Golberg, *Chem. Phys. Lett.*, 2003, **372**, 635.
123 D. W. He, F. X. Zhang, X. Y. Zhang, Z. C. Qin, M. Zhang, R. P. Liu, Y. F. Xu and W. K. Wang, *J. Mater. Res.*, 1998, **13**, 3458.
124 A. J. Stewens, T. Koga, C. B. Agee, M. J. Aziz and C. M. Lieber, *J. Am. Chem. Soc.*, 1996, **118**, 10900.
125 J. V. Badding and D. C. Nesting, *Chem. Mater.*, 1996, **8**, 1535.
126 D. C. Nesting, J. Kouvetakis and J. V. Badding, *Adv. Mater.-98, Proc. Int. Symp. 5th, (ISAM '98)*, National Institute for Research in Inorganic Materials, Tsukuba, Japan, 1998, pp. 1–4.
127 J. H. Nguyen and R. Jeanloz, *Mater. Sci. Eng., A*, 1996, **209**, 23.
128 V. L. Solozhenko, E. G. Solozhenko and C. Lathe, *J. Superhard Mater.*, 2002, **24**, 95.
129 V. L. Solozhenko, E. G. Solozhenko, P. V. Zinin, L. C. Ming, J. Chen and J. B. Parise, *J. Phys. Chem.*, 2003, **64**, 1265.
130 Komatsu Tamikuni, *Jpn. Pat.*, P2000-51678A, 2000.
131 V. N. Khabasheku and J. L. Margrave, *Adv. Eng. Mater.*, 2002, **4**, 671.
132 Y. H. Han, J. F. Luo, C. X. Gao, H. A. Ma, A. M. Hao, Y. C. Li, X. D. Li, J. Liu, M. Li, H. W. Liu and G. T. Zuo, *Chin. Phys. Lett.*, 2005, **22**, 1347.
133 K. Kollisch and W. Schnick, *Angew. Chem., Int. Ed.*, 1999, **38**, 357.
134 K. Leinenweber, M. O'Keeffe, M. Somayazulu, H. Hubert, P. F. McMillan and G. H. Wolf, *Chem.–Eur. J.*, 1999, **5**, 3076–3080.
135 G. Serghiou, G. Miehe, O. Tschauner, A. Zerr and R. Boehler, *J. Chem. Phys.*, 1999, **111**, 4659.
136 A. Zerr, G. Miehe, G. Serghiou, M. Schwarz, E. Kroke, R. Riedel and R. Boehler, *Proc. AIRAPT Conf. High-Pressure Sci. Technol., 17th*, ed. M. H. Manghnani, W. J. Nellis and M. F. Nicol, Universities Press, Hyderabad, India, 2000, pp. 914–917.
137 E. Soignard and P. F. McMillan, *Chem. Mater.*, 2004, **16**, 3533–3542.
138 M. Schwarz, G. Miehe, A. Zerr, E. Kroke, B. Poe, H. Fuess, D. C. Rubie and R. Riedel, *Adv. Mater.*, 2000, **12**, 883.
139 H. He, T. Sekine, T. Kobayashi and K. Kimoto, *J. Appl. Phys.*, 2001, **90**, 4403.
140 N. Scotti, W. Kockelmann, J. Senker, S. Trabel and H. Jacobs, *Z. Anorg. Allg. Chem.*, 1999, **62**, 1435–1439.
141 M. P. Shemkunas, G. H. Wolf, K. Leinenweber and W. T. Petuskey, *J. Am. Ceram. Soc.*, 2002, **85**, 101–104.
142 S. Nishikawa, *Proc. Math. Phys. Soc. Tokyo*, 1915, **8**, 199.
143 K. E. Sickafus, J. M. Wills and N. G. Grimes, *J. Am. Ceram. Soc.*, 1999, **82**, 3279.
144 J. Z. Jiang, F. Kragh, D. J. Frost, K. Stahl and H. Lindelov, *J. Phys.: Condens. Matter*, 2001, **13**, L515.
145 T. Sekine and T. Mitsuhashi, *Appl. Phys. Lett.*, 2001, **79**, 2719.
146 E. Soignard, M. Somayazulu, J. Dong, O. F. Sankey and P. F. McMillan, *J. Phys.: Condens. Matter*, 2001, **13**, 557.
147 A. Zerr, M. Kempf, M. Schwarz, E. Kroke, M. Goken and R. Riedel, *J. Am. Ceram. Soc.*, 2002, **85**, 86.
148 J. Dong, O. F. Sankey, S. K. Deb, G. H. Wolf and P. F. McMillan, *Phys. Rev. B: Condens. Matter Mater. Phys.*, 2000, **61**, 11979.
149 S. Leitch, A. Moewes, L. Ouyang, W. Y. Ching and T. Sekine, *J. Phys.: Condens. Matter*, 2004, **16**, 6469.
150 S. D. Mo, *Phys. Rev. Lett.*, 1999, **83**, 5046.
151 B. Molina and L. E. Sansores, *Int. J. Quantum Chem.*, 2003, **80**, 249.
152 A. Zerr, *Phys. Status Solidi B*, 2001, **227**, R4.
153 M. P. Shemkunas, W. P. Petuskey, A. V. G. Chizmeshya, K. Leinenweber and G. H. Wolf, *J. Mater. Res.*, 2004, **19**, 1392.
154 H. He, T. Sekine, T. Kobayashi, H. Hirosaki and I. Suzuki, *Phys. Rev. B: Condens. Matter Mater. Phys.*, 2000, **62**, 11412.
155 T. Sekine, H. He, T. Kobayashi, M. Zhang and F. Xu, *Appl. Phys. Lett.*, 2000, **76**, 3706.
156 S. N. Ruddlesden and P. Popper, *Acta Crystallogr.*, 1958, **11**, 465.

157 E. Soignard, P. F. McMillan, C. Hejny and K. Leinenweber, *J. Solid State Chem.*, 2004, **177**, 299–311.
158 F. Munakata, K. Matsuo, K. Furuya, Y. J. Akimune and I. Ishikawa, *Appl. Phys. Lett.*, 1999, **74**, 3498.
159 A. R. Zanatta and L. A. O. Nunes, *Appl. Phys. Lett.*, 1998, **72**, 3127.
160 Y. Duan, K. Zhang and X. Xie, *Phys. Status Solidi B*, 1997, **200**, 499.
161 W. Y. Ching and P. Rulis, *Phys. Rev. B: Condens. Matter Mater. Phys.*, 2006, **73**, 045202.
162 J. Z. Jiang, H. Lindelov, L. Gerward, K. Stahl, J. M. Recio, P. Mori-Sánchez, S. Carlson, M. Mezouar, E. Dooryhee, A. Fitch and D. J. Frost, *Phys. Rev. B: Condens. Matter Mater. Phys.*, 2002, **65**, 161202.
163 W. Paszkowicz, R. Minikayev, P. Piszora, M. Knapp, C. Bähtz, J. M. Recio, M. Marquès, P. Mori-Sánchez, L. Gerward and J. Z. Jiang, *Phys. Rev. B: Condens. Matter Mater. Phys.*, 2004, **69**, 052103.
164 E. Soignard, M. Somayazulu, H. K. Mao, J. Dong, O. F. Sankey and P. F. McMillan, *Solid State Commun.*, 2001, **120**, 237.
165 E. Soignard, P. F. McMillan and K. Leinenweber, *Chem. Mater.*, 2004, **16**, 5344.
166 J. Dong, J. Deslippe, O. F. Sankey, E. Soignard and P. F. McMillan, *Phys. Rev. B: Condens. Matter Mater. Phys.*, 2003, **64**, 094104.
167 R. Riedel, A. Greiner, G. Miehe, W. Dressler, H. Fuess, J. Bill and F. Aldinger, *Angew. Chem., Int. Ed. Engl.*, 1997, **36**, 603.
168 R. Riedel, E. Kroke, A. Greiner, A. O. Gabriel, L. Ruwisch and J. Nicolich, *Chem. Mater.*, 1998, **10**, 2964.
169 P. Kroll, *J. Solid State Chem.*, 2003, **176**, 530.
170 J. E. Lowther, *Phys. Rev. B: Condens. Matter Mater. Phys.*, 1999, **60**, 11943.
171 J. E. Lowther, M. Amkreutz, T. Frauenheim, E. Kroke and R. Riedel, *Phys. Rev. B: Condens. Matter Mater. Phys.*, 2003, **68**, 0332011.
172 B. Amadon and F. Finocchi, *Eur. Phys. J. B*, 1999, **11**, 207.
173 V. L. Solozhenko, M. Schwarz and R. Riedel, *Solid State Commun.*, 2004, **132**, 573.
174 R. Juza, A. Rabenau and I. Nitschke, *Z. Anorg. Allg. Chem.*, 1964, **332**, 1.
175 A. Yajima, Y. Segawa, R. Matsuzaki and Y. Saeki, *Bull. Chem. Soc. Jpn.*, 1983, **56**, 2638.
176 M. Lerch, E. Füglein and J. Wrba, *Z. Anorg. Allg. Chem.*, 1996, **622**, 367.
177 W. Y. Ching, S.-D. Mo, L. Ouyang, I. Tanaka and M. Yoshiya, *Phys. Rev. B: Condens. Matter Mater. Phys.*, 2000, **61**, 10609.
178 W. Y. Ching, S.-D. Mo, I. Tanaka and M. Yoshiya, *Phys. Rev. B: Condens. Matter Mater. Phys.*, 2001, **63**, 064102.
179 W. Y. Ching, S.-D. Mo, L. Ouyang, P. Rulis, I. Tanaka and M. Yoshiya, *J. Am. Ceram. Soc.*, 2002, **85**, 75.
180 W. Y. Ching, Y.-N. Xu and L. Ouyang, *Phys. Rev. B: Condens. Matter Mater. Phys.*, 2002, **66**, 235106.
181 E. Soignard, P. F. McMillan, T. D. Chaplin, S. M. Farag, C. . Bull, M. S. Somayazulu and K. Leinenweber, *Phys. Rev. B: Condens. Matter Mater. Phys.*, 2003, **68**, 132101.
182 E. Gregoryanz, C. Sanloup, M. Somayazulu, J. Badro, G. Fiquet, H. K. Mao and R. J. Hemley, *Nat. Mater.*, 2004, **3**, 294.
183 J. C. Crowhurst, A. F. Goncharov, B. Sadigh, C. L. Evans, P. G. Morrall, J. L. Ferreira and A. J. Nelson, *Science*, 2006, **311**, 1275.
184 J. Li, D. Dzivenko, A. Zerr, C. Fasel, Y. Zhou and R. Riedel, *Z. Anorg. Allg. Chem.*, 2005, **631**, 1449.
185 R. Fix, R. G. Gordon and D. M. Hoffman, *Chem. Mater.*, 1991, **3**, 1138.
186 D. A. Dzivenko, A. Zerr, V. K. Bulatov, J. Brötz, B. Thybusch, H. Fuess, G. Brey and R. Riedel, unpublished work.
187 B. R. Sahu and L. Kleinman, *Phys. Rev. B: Condens. Matter Mater. Phys.*, 2005, **71**, 041101(R).
188 B. R. Sahu and L. Kleinman, *Phys. Rev. B: Condens. Matter Mater. Phys.*, 2005, **72**, 119901.
189 J. Uddin and G. E. Scuseria, *Phys. Rev. B: Condens. Matter Mater. Phys.*, 2005, **72**, 035101.
190 J. Uddin and G. E. Scuseria, *Phys. Rev. B: Condens. Matter Mater. Phys.*, 2005, **72**, 119902.
191 R. Yu and X. F. Zhang, *Appl. Phys. Lett.*, 2005, **86**, 121913.
192 C.-Z. Fan, L.-L. Sun, Y.-X. Wang, Z.-J. Wei, R.-P. Liu, S.-Y. Zeng and W.-K. Wang, *Chin. Phys. Lett.*, 2005, **22**, 2637.
193 V. L. Solozhenko and E. Gregoryanz, *Mater. Today*, 2005, 44.
194 M. Hasegawa and T. Yagi, *Solid State Commun.*, 2005, **135**, 294.
195 M. Hasegawa and T. Yagi, *J. Alloys Compd.*, 2005, **403**, 131.
196 M. Mattesini, R. Ahuja and B. Johansson, *Phys. Rev. B: Condens. Matter Mater. Phys.*, 2003, **68**, 184108.
197 P. Kroll, *Phys. Rev. Lett.*, 2003, **90**, 125501.
198 D. A. Dzivenko, A. Zerr, R. Boehler and R. Riedel, *Solid State Commun.*, 2006, **139**, 255.
199 M. Chhowalla and H. E. Unalan, *Nat. Mater.*, 2005, **4**, 317.
200 J. C. Crowhurst, A. F. Goncharov, J. L. Ferreira, C. L. Evans and J. M. Zaug, in *Joint 20th AIRAPT–43rd EHPRG Int. Conf. High Pressure Sci. Technol.*, ed. E. Dinjus and N. Dahmen, Forschungszentrum Karlsruhe GmbH, Karlsruhe, Germany, 2005.
201 E. Gregoryanz, C. Sanloup, A. Young, M. Somayazulu, H. K. Mao and R. J. Hemley, in *Joint 20th AIRAPT–43rd EHPRG Int. Conf. High Pressure Sci. Technol.*, ed. E. Dinjus and N. Dahmen, Forschungszentrum Karlsruhe GmbH, Karlsruhe, Germany, 2005; A. F. Young, C. Sanloup, E. Gregoryanz, R. J. Hemley and H. K. Mao, *Phys. Rev. Lett.*, 2006, **96**, 155501.
202 W. Lengauer, Transition Metal Carbides, Nitrides, and Carbonitrides, in *Handbook of Ceramic Hard Materials, 1*, ed. R. Riedel, Wiley-VCH, Weinheim, 2000, pp. 202–252.
203 S. T. Oyoma, *The Chemistry of Transition Metal Carbides and Nitrides*, Blackie Academic & Professional, Glasgow, 1996.
204 L. E. Toth, *Transition Metal Carbides and Nitrides*, Academic Press, New York, 1971.
205 A. Bezinge, K. Yvon, J. Muller, W. Lengauer and P. Ettmayer, *Solid State Commun.*, 1987, **63**, 141.
206 C. L. Bull, P. F. McMillan, E. Soignard and K. Leinenweber, *J. Solid State Chem.*, 2004, **177**, 1488.
207 T. Chen, X. Yang, P. Sourivong, K. Kamimura, A. J. Viescas, C. J. Yen Chen, J. D. Curley, D. J. Phares, H. E. Hall, P. A. Dayton, C. B. Hart and J. T. Wang, *Phys. Lett. A*, 1996, **17**, 167.
208 X.-J. Chen, V. V. Struzhkin, Z. Wu, M. Somayazulu, J. Qian, S. Kung, A. N. Christensen, Y. Zhao, R. E. Cohen, H. Mao and R. J. Hemley, *Proc. Natl. Acad. Sci. U. S. A.*, 2005, **102**, 3198.
209 J. K. Hulm, M. S. Walker and N. Pessall, *Physica*, 1971, **55**, 60.
210 D. A. Papaconstantopolous, W. E. Pickett, B. M. Klein and L. L. Boyer, *Phys. Rev. B: Condens. Matter*, 1985, **31**, 752.
211 R. Riedel, *Handbook of Ceramic Hard Materials*, Wiley-VCH, Weinheim, 2000.
212 W. Schnick, *Angew. Chem., Int. Ed. Engl.*, 1993, **32**, 806.
213 L. S. Dubrovinsky, N. A. Dubrovinskaia, V. Swamy, J. Muscat, R. Harrison, B. Ahuja, B. Holm and B. Johansson, *Nature*, 2001, **410**, 653.
214 J. Haines, J. M. Léger and G. Bocquillon, *Ann. Rev. Mater. Res.*, 2001, **31**, 1.
215 U. Lundin, L. Fast, L. Nordström and B. Johansson, *Phys. Rev. B: Condens. Matter Mater. Phys.*, 1998, **57**, 4979.
216 J. Dong, A. A. Kinkhabwala and P. F. McMillan, *Phys. Status Solidi B*, 2004, **241**, 2319.
217 P. Kroll and W. Schnick, *Angew. Chem., Int. Ed.*, 2002, **8**, 3530.
218 K. Landskron, H. Huppertz, J. Senker and W. Schnick, *Angew. Chem., Int. Ed.*, 2001, **40**, 2643.
219 Editorial, Ceramics based on silicon-nitride, *Nature*, 1972, **238**, 128.
220 M. Herrmann, H. Klemm and C. Schubert, Silicon Nitride Based Hard Materials, in *Handbook of Ceramic Hard Materials, 2*, ed. R. Riedel, Wiley-VCH, Weinheim, 2000, pp. 749–801.
221 K. H. Jack, *Trans. J. Br. Ceram. Soc.*, 1973, **19**, 376.
222 K. H. Jack, *J. Mater. Sci.*, 1976, **11**, 1135.
223 K. H. Jack, *Mater. Res. Bull.*, 1978, **13**, 1327.
224 P. L. Land, J. M. Wimmer, R. W. Burns and N. S. Choudhury, *J. Am. Ceram. Soc.*, 1978, **61**, 56.
225 M. H. Lewis, B. D. Powell, P. Drew, R. J. Lumby, B. North and A. J. Taylor, *J. Mater. Sci.*, 1977, **12**, 61.
226 M. H. Lewis and R. J. Lumby, *Powder Metal. Met. Ceram.*, 1983, **26**, 73.
227 M. Mitomo, N. Kuramoto and Y. Inomata, *J. Mater. Sci.*, 1979, **14**, 2309.
228 C. C. Sorrell, *J. Aust. Ceram. Soc.*, 1983, **19**, 48.

 

229 L. Gillott, N. Cowlam and G. E. Bacon, *J. Mater. Sci.*, 1981, **16**, 2263.
230 F. K. van Dijen, R. Metselaar and R. B. Helmholdt, *J. Mater. Sci. Lett.*, 1987, **6**, 1101.
231 R. Marchand, Y. Laurent, J. Guyader, P. l'Haridon and P. Verdier, *J. Eur. Ceram. Soc.*, 1991, **8**, 197.
232 R. Metselaar, *Pure Appl. Chem.*, 1994, **66**, 1815.
233 P. F. McMillan, R. K. Sato and B. T. Poe, *J. Non-Cryst. Solids*, 1998, **224**, 267.
234 H. Lemercier, T. Rouxel, D. Fargeot, J.-L. Besson and B. Piriou, *J. Non-Cryst. Solids*, 1996, **201**, 128.
235 J. W. McCauley and N. D. Corbin, *J. Am. Ceram. Soc.*, 1979, **62**, 476.
236 M. Schwarz, A. Zerr, E. Kroke, G. Miehe, I.-W. Chen, M. Heck, B. Thybusch, B. T. Poe and R. Riedel, *Angew. Chem., Int. Ed.*, 2002, **41**, 789.
237 J. E. Lowther, T. Wagner, I. Kinski and R. Riedel, *J. Alloys Compd.*, 2004, **376**, 1.
238 M. Puchinger, D. J. Kisailus, E. F. Lange and T. Wagner, *J. Cryst. Growth*, 2002, **245**, 219.
239 S. D. Wolter, J. M. DeLucca, S. E. Mohney, R. S. Kern and C. P. Kuo, *Thin Solid Films*, 2000, **371**, 153.
240 I. Kinski, G. Miehe, G. Heymann, R. Theissmann, R. Riedel and H. Huppertz, *Z. Naturforsch., B: Chem. Sci.*, 2005, **60**, 831.
241 E. Soignard, D. Machon, P. F. McMillan, J. Dong, B. Xu and K. Leinenweber, *J. Chem. Mater.*, 2005, **17**, 5465.
242 L. Cartz and J. D. Jorgensen, *J. Appl. Phys.*, 1981, **52**, 236.
243 P. Kroll and M. Milko, *Z. Anorg. Allg. Chem.*, 2003, **629**, 1737.
244 T. Sekine, H. He, T. Kobayashi and K. Shibata, *Am. Mineral.*, 2006, **91**, 463.
245 T. Sekine, X. Li, T. Kobayashi and Y. Yamashita, *J. Appl. Phys.*, 2003, **94**, 4803.
246 A. I. Balabanovich, S. V. Levchik, G. F. Levchik, W. Schnabel and C. A. Wilkie, *Polym. Degrad. Stab.*, 1999, **64**, 191.
247 H. Hbib and O. Bonnaud, *Philos. Mag. Lett.*, 1997, **75**, 111.
248 H. Hbib, O. Bonnaud, M. Gauneau, L. Hamedi, R. Marchand and A. Quemerais, *Thin Solid Films*, 1997, **310**, 1.
249 E. D. Weil and N. G. Patel, *Fire Mater.*, 1994, **18**, 1.
250 E. V. Borisov and E. E. Nifant'ev, *Russ. Chem. Rev.*, 1977, **46**, 842.
251 S. Horstmann, E. Irran and W. Schnick, *Angew. Chem., Int. Ed. Engl.*, 1997, **36**, 1873.
252 W. Schnick, J. Lucke and F. Krumeich, *Chem. Mater.*, 1996, **8**, 281.
253 S. Horstmann, E. Irran and W. Schnick, *Angew. Chem., Int. Ed. Engl.*, 1997, **36**, 1992.
254 L. Boukbir, R. Marchand, Y. Laurent, P. Bacher and G. Roult, *Ann. Chim. (Paris)*, 1989, **14**, 475.
255 C. Chateau, J. Haines, J. M. Léger, A. Lesauze and R. Marchand, *Am. Mineral.*, 1999, **84**, 207.
256 J. Haines, C. Chateau, J. M. Léger, A. Lesauze, N. Diot, R. Marchand and S. Hull, *Acta Crystallogr., Sect. B: Struct. Sci.*, 1999, **55**, 677.
257 J. M. Léger, J. Haines, C. Chateau, G. Bocquillon, M. W. Schmidt, S. Hull, F. Gorelli, A. Lesauze and R. Marchand, *Phys. Chem. Miner.*, 2001, **28**, 388.
258 G. Miehe and H. Graetsch, *Eur. J. Mineral.*, 1992, **4**, 693.
259 J. M. Léger, J. Haines, L. S. de Oliveira, C. Chateau, A. Lesauze and R. Marchand, *C. R. Acad. Sci., Ser. IIc: Chim.*, 1998, **1**, 237.
260 K. J. Kingma, R. E. G. Pacalo and P. F. McMillan, *Eur. J. Solid State Inorg. Chem.*, 1997, **34**, 679.
261 K. J. Kingma, R. E. G. Pacalo and P. F. McMillan, Compression of PON cristobalite to 70 GPa., in *Properties of Earth and Planetary Materials*, ed. Y. Syono and M. H. Manghnani, American Geophysical Union, Washington DC, 1998, pp. 105–117.
262 J. M. Léger, J. Haines and C. Chateau, *Eur. J. Mineral.*, 2001, **13**, 351.
263 J. M. Léger, J. Haines, C. Chateau and R. Marchand, *J. Phys. Chem. Solids*, 2000, **61**, 1447.
264 J. M. Léger, J. Haines, L. S. de Oliveira, C. Chateau, A. Lesauze and R. Marchand, *J. Phys.: Condens. Matter*, 1996, **8**, L773.
265 H. Jacobs, R. Nymwegen, S. Doyle, T. Wroblewski and W. Kockelman, *Z. Anorg. Allg. Chem.*, 1997, **623**, 1467.
266 B. Bunker, D. R. Tallant, C. A. Balfe, R. J. Kirkpatrick, G. L. Turner and M. R. Reidmeyer, *J. Am. Ceram. Soc.*, 1987, **70**, 675.
267 M. R. Reidmeyer and D. E. Day, *J. Non-Cryst. Solids*, 1995, **181**, 201.
268 T. Grande, J. R. Holloway, P. F. McMillan and C. A. Angell, *Nature*, 1994, **369**, 43.
269 T. Grande, S. Jacob, J. R. Holloway, P. F. McMillan and C. A. Angell, *J. Non-Cryst. Solids*, 1995, **184**, 151.
270 B. T. Poe, D. C. Rubie, S. Chakraborty, J. Yarger, J. Diefenbacher and P. F. McMillan, *Science*, 1997, **276**, 1245.
271 G. H. Wolf and P. F. McMillan, *Rev. Mineral.*, 1995, **32**, 505.
272 J. L. Yarger, K. H. Smith, R. A. Nieman, J. Diefenbacher, G. H. Wolf, B. T. Poe and P. F. McMillan, *Science*, 1995, **270**, 1964.
273 A. D. Mazzoni, M. S. Conconi and E. F. Aglietti, *Mater. Res.*, 2001, **4**, 107.
274 C. M. Fang, E. Orhan, G. A. Wiks, H. T. Hintzen, R. A. de Groot, R. Marchand, J. –Y. Saillard and G. de With, *J. Mater. Chem.*, 2001, **11**, 1248.
275 X. Z. Chen and H. A. Eick, *J. Solid State Chem.*, 1996, **127**, 19.
276 S. Esmaeilzadeh and W. Schnick, *Solid State Sci.*, 2003, **5**, 503.
277 R. Niewa and H. Jacobs, *J. Alloys Compd.*, 1995, **217**, 38.
278 R. Niewa and H. Jacobs, *Chem. Rev.*, 1996, **96**, 2053.
279 R. Assabaa-Boultif, R. Marchand, Y. Laurent and Y. Eu, *J. Solid State Inorg. Chem.*, 1995, **32**, 1101.
280 N. Brese and F. J. DiSalvo, *J. Solid State Chem.*, 1995, **120**, 372.
281 S. H. Elder, F. J. DiSalvo, J. B. Parise, J. A. Hrijlac and J. W. Richardson, *J. Solid State Chem.*, 1994, **108**, 73.
282 S. H. Elder, F. J. DiSalvo, L. Topor and A. Navrotsky, *Chem. Mater.*, 1993, **5**, 1545.
283 I. D. Fawcett, K. V. Ramanujachary and M. Greenblatt, *Mater. Res. Bull.*, 1997, **32**, 1565.
284 F. Tessier, R. Assabaa and R. Marchand, *J. Alloys Compd.*, 1997, **262–263**, 512.
285 M. Lerch, E. Fuglein, J. Wrba and Z. Anorg, *Allg. Chem.*, 1996, **622**, 367.
286 G. Auffermann, Yu. Prots and R. Kniep, *Angew. Chem., Int. Ed.*, 2001, **40**, 565.
287 Yu. Prots, G. Auffermann, M. Tovar and R. Kniep, *Angew. Chem., Int. Ed.*, 2002, **41**, 2288.
288 R. Kniep, Yu. Prots and G. Auffermann, to be published.
289 G. V. Vajenine, G. Auffermann, Yu. Prots, W. Schnelle, R. K. Kremer, A. Simon and R. Kniep, *Inorg. Chem.*, 2001, **40**, 4866.
290 G. Auffermann, U. Schmidt, B. Bayer, Yu. Prots and R. Kniep, *Anal. Bioanal. Chem.*, 2002, **373**, 880.
291 G. Auffermann, Yu. Prots, R. Kniep, S. F. Parker and S. M. Bennington, *ChemPhysChem*, 2002, **3**, 815.
292 A. K. McMahan and R. LeSar, *Phys. Rev. Lett.*, 1985, **54**, 1929.
293 C. Mailhiot, L. H. Yang and A. K. McMahan, *Phys. Rev. B: Condens. Matter*, 1992, **46**, 14419.
294 M. I. Eremets, A. G. Gavriliuk, I. A. Trojan, D. A. Dzivenko and R. Boehler, *Nat. Mater.*, 2004, **3**, 558.
295 G. Kresse and J. Hafner, *Phys. Rev. B: Condens. Matter*, 1993, **47**, 558; G. Kresse and J. Hafner, *Phys. Rev. B: Condens. Matter*, 1994, **49**, 14251.
296 G. Kresse and J. Furthmüller, *Comput. Mater. Sci.*, 1996, **6**, 15.
297 G. Kresse and J. Furthmüller, *Phys. Rev. B: Condens. Matter*, 1996, **54**, 11169.
298 P. E. Blöchl, *Phys. Rev. B: Condens. Matter*, 1994, **50**, 17953.
299 G. Kresse and D. Joubert, *Phys. Rev. B: Condens. Matter Mater. Phys.*, 1999, **59**, 1758.
300 N. Funamori, R. Jeanloz, J. H. Nguyen, A. Kavner, W. A. Caldwell, K. Fujino, N. Miyajima, T. Shinmei and N. Tomioka, *J. Geophys. Res., [Solid Earth]*, 1998, **103**, 20813.
301 C. Haavik, S. Stolen, H. Fjellvag, M. Hanfland and D. Hausermann, *Am. Mineral.*, 2000, **85**, 514.
302 P. Kroll and J. von Appen, *Phys. Status Solidi B*, 2001, **226**, R6.
303 T. Sekine, talk presented at *2nd Workshop on Spinel Nitrides and Related Materials*, Rüdesheim, Germany, 2004.
304 P. Kroll, *J. Solid State Chem.*, 2003, **76**, 530.
305 T. Sekine, *J. Am. Ceram. Soc.*, 2002, **85**, 113.
306 P. Kroll and W. Schnick, *Chem.–Eur. J.*, 2002, **8**, 3530.
307 J.-J. Dong, *Phys. Status Solidi B*, 2004, **241**, 2319.

308 P. Kroll, *Phys. Rev. Lett.*, 2003, **90**, 125501.
309 P. Kroll, *J. Phys.: Condens. Matter*, 2004, **16**, S1235.
310 P. Kroll, T. Schroeter and M. Peters, *Angew. Chem., Int. Ed.*, 2005, **44**, 4249.
311 R. J. Meyer, F. Peters, L. Gmelin, E. Pietsch and M. Becke-Goehring, in *Gmelin's Handbuch der Anorganischen Chemie*, System 54, Verlag Chemie, Berlin, 8th edn, 1933, pp. 153.
312 J.-C. Gilles, *C. R. Seances Acad. Sci., Ser. C*, 1968, **266**, 546.
313 M. W. Chase, JANAF-Thermochemical Tables, *J. Phys. Chem. Ref. Data*, 1998, Monograph 9.
314 R. T. Jacobsen, R. B. Stewart and M. Jahangiri, *J. Phys. Chem. Ref. Data*, 1986, **15**, 735.
315 J. Unland, B. Onderka, A. Davydov and R. Schmid-Fetzer, *J. Cryst. Growth*, 2003, **256**, 33.
316 M. Hasegawaa and T. Yagi, *Solid State Commun.*, 2005, **135**, 294.



 